haematologica
Journal of the Ferrata Storti Foundation

Combinatorial strategies targeting NEAT1 and AURKA as new potential therapeutic options for multiple myeloma

by Noemi Puccio, Gloria Manzotti, Elisabetta Mereu, Federica Torricelli, Domenica Ronchetti, Michela Cumerlato, Ilaria Craparotta, Laura Di Rito, Marco Bolis, Valentina Traini, Veronica Manicardi, Valentina Fragliasso, Yvan Torrente, Nicola Amodio, Niccolo Bolli, Elisa Taiana, Alessia Ciarrocchi, Roberto Piva, and Antonino Neri

Received: March 22, 2024.
Accepted: July 2, 2024.

Citation: Noemi Puccio, Gloria Manzotti, Elisabetta Mereu, Federica Torricelli, Domenica Ronchetti, Michela Cumerlato, Ilaria Craparotta, Laura Di Rito, Marco Bolis, Valentina Traini, Veronica Manicardi, Valentina Fragliasso, Yvan Torrente, Nicola Amodio, Niccolo Bolli, Elisa Taiana, Alessia Ciarrocchi, Roberto Piva, and Antonino Neri. Combinatorial strategies targeting NEAT1 and AURKA as new potential therapeutic options for multiple myeloma.
Haematologica. 2024 July 11. doi: 10.3324/haematol.2024.285470 [Epub ahead of print]

Combinatorial strategies targeting NEAT1 and AURKA as new potential therapeutic options for multiple myeloma.

Authors:

Noemi Puccio[1,2], Gloria Manzotti[1], Elisabetta Mereu[3], Federica Torricelli[1], Domenica Ronchetti[4], Michela Cumerlato[3], Ilaria Craparotta[5], Laura Di Rito[5], Marco Bolis[5,6], Valentina Traini[4], Veronica Manicardi[1], Valentina Fragliasso[1], Yvan Torrente[7], Nicola Amodio[8], Niccolò Bolli[4,9], Elisa Taiana[9], Alessia Ciarrocchi[1], Roberto Piva[3], Antonino Neri[10].

[1]Laboratory of Translational Research, Azienda USL-IRCCS di Reggio Emilia, Reggio Emilia; [2]Clinical and Experimental Medicine PhD Program, University of Modena and Reggio Emilia, Modena; [3]Department of Molecular Biotechnology and Health Sciences, University of Turin, Turin, Italy; [4]Department of Oncology and Hemato-Oncology, University of Milan, Milan, Italy; [5]Computational Oncology Unit, Oncology Department, Mario Negri IRCCS, Milan; [6]Bioinformatics Core Unit, Institute of Oncology Research (IOR), Bellinzona, Switzerland; [7]Stem Cell Laboratory, Department of Pathophysiology and Transplantation, University of Milan, Centro Dino Ferrari, Unit of Neurology, Fondazione IRCCS Cà Granda Ospedale Maggiore Policlinico, 20122 Milan, Italy; Novystem Spa, Milan; [8]Department of Experimental and Clinical Medicine, Magna Graecia University of Catanzaro, Catanzaro; [9]Hematology Unit, Fondazione IRCCS Cà Granda Ospedale Maggiore Policlinico, Milan, Italy; [10]Scientific Directorate, Azienda USL-IRCCS di Reggio Emilia, 42123 Reggio Emilia, Italy.

Correspondence: Antonino Neri, MD

Azienda USL-IRCCS Reggio Emilia, viale Umberto I 50, 42123 Reggio Emilia, Italy

Phone: 0522 296979; Fax: 0522 295622

mail: antonino.neri@ausl.re.it

Running Title: AURKA and NEAT1 cooperate to support MM pathogenesis.

Data-sharing statement: Data are available at ArrayExpress; access code: E-MTAB-13925.

Funding:

This work was supported by Fondazione AIRC, IG-24365 (AN), MFAG 2022-ID.27606 (ET), MFAG 2023-ID. 28974 (VF), IG-24449 (NA), IG21585 (RP), NB is funded by the European Research Council under the European Union's Horizon 2020 research and innovation program (grant agreement no. 817997).

NP received a fellowship by the PhD program in Clinical and Experimental Medicine of University of Modena and Reggio Emilia. VT received a fellowship by the PhD program in Experimental Medicine of the University of Milan.

Acknowledgements

YT acknowledges support by "Piattaforme cellulari per la Ricerca e lo Sviluppo di Terapie Avanzate in Life Science" - Fondo Europeo di Sviluppo Regionale 2014-2020. POR FESR 2014-2020. IC and LR acknowledges the CINECA award under the ISCRA and ELIXIR-IV initiative, for the availability of high-performance computing resources and support.

Author Contributions NP, GM, IC, LR, MB, VM, VF performed experiments and analyzed the data; FT and DR performed CoMMpass analysis, EM and MC performed highthroughput experiments; NP performed live cell-imaging experiments, NP, ET, VT performed confocal experiments; ET, YT, NA, NB, RP, provided critical evaluation of experimental data and of the manuscript. NP, AC and AN conceived the study and wrote the manuscript.

Disclosures. The authors declare no conflicts of interest

ABSTRACT

Multiple myeloma (MM) is a dreadful disease, marked by the uncontrolled proliferation of clonal plasma cells (PCs) within the bone marrow (BM). MM is characterized by a highly heterogeneous clinical and molecular background, supported by severe genomic alterations. Important de-regulation of long non-coding RNAs (lncRNAs) expression has been reported in MM patients, influencing progression and therapy resistance. NEAT1 is a lncRNA essential for nuclear paraspeckles and involved in gene expression regulation. We showed that NEAT1 supports MM proliferation making this lncRNA an attractive therapeutic candidate.

Here, we used a combinatorial strategy integrating transcriptomic and computational approaches with functional high-throughput drug screening, to identify compounds that synergize with NEAT1 inhibition in restraining MM cells growth. AUKA inhibitors were identified as top-scoring drugs in these analyses. We showed that the combination of NEAT1 silencing and AURKA inhibitors in MM profoundly impairs microtubule organization and mitotic spindle assembly, finally leading to cell death. Analysis of the large publicly CoMMpass dataset showed that in MM patients AURKA expression is strongly associated with reduced progression-free ($p < 0.0001$) and overall survival probability ($p < 0.0001$) and patients displaying high expression levels of both NEAT1 and AURKA have a worse clinical outcome. Finally, using RNA-sequencing data from NEAT1 knockdown (KD) MM cells, we identified the AURKA allosteric regulator TPX2 as a new NEAT1 target in MM and as a mediator of the interplay between AURKA and NEAT1, therefore providing a possible explanation of the synergistic activity observed upon their combinatorial inhibition.

INTRODUCTION

Multiple myeloma (MM) is an incurable bone marrow-resident hematological malignancy, characterized by an uncontrolled proliferation of clonal plasma cells (PCs)[1]. It is the second most common type of blood cancer, after non-Hodgkin Lymphoma, representing 10% of all hematological tumors[2]. MM presents a highly heterogeneous clinical and genetic background, characterized by both numerical and structural chromosomal abnormalities and gene mutations[3,4].

Long non-coding RNAs (lncRNAs) represent a heterogeneous class of transcripts that partake in all levels of genome organization[5]. These molecules are involved in the regulation of cell differentiation, development, response to DNA damage and regulation of metabolic processes. In cancer, lncRNAs contribute to altering cell growth potential, invasion and metastatic ability, to impair cell death mechanisms, and to increase anti-tumor drug resistance[6,7]. Due to their biological relevance, it is not surprising that these molecules are regarded as new potential targets for innovative cancer treatments.

In MM, lncRNAs expression profile was described to be significantly different between malignant and normal PCs, suggesting their pro-oncogenic function in this scenario[8]. Aberrant lncRNAs expression in myeloma cells can further contribute to the acquisition of genomic instability (GI), inducing cell transcriptome modification and interfering with chromatin structure[9,10].

NEAT1 is a mono-exonic lncRNA transcribed from the MEN type I locus, localized on human chromosome 11q13. NEAT1 gene produces two different isoforms that share the same 5' terminus: a short and polyadenylated isoform (NEAT1_1) and a longer one (NEAT1_2) lacking a poly-A tail but endowed with a triple-helix structure that protects the transcript from degradation[11,12]. As in other types of cancer, increased NEAT1 expression has been shown to be a hallmark of MM and plasma cell leukemia[13].

NEAT1 mainly localizes in cell nuclei. The long NEAT1 isoform (NEAT1_2) acts as an essential architectural scaffold for stress-induced paraspeckles (PSs)[14]. PSs are sub-nuclear membranelles organelles that regulate gene expression through three main mechanisms: by acting as RNA binding proteins hub, miRNA sponge, and promoting mRNA retention[15–17]. By contrast, the short NEAT1 (NEAT1_1) is the most abundant isoform but it is dispensable for PSs assembly and functioning, suggesting a putative independent role[18]. It has been already proved that NEAT1 is required to support MM cells proliferation and viability, both *in vitro* and *in vivo*[19-20]. In line with this observation, NEAT1 silencing causes a decreased resistance to standard myeloma treatments such as Bortezomib, Carfilzomib and Melphalan and improves Olaparib sensitivity, making this lncRNA an attractive candidate for the development of novel anti-myeloma strategies[19].

In this work, we took advantage of an integrated approach combining computational predictive tools with a high throughput functional screening to identify small compounds that cooperate with NEAT1 inhibition in bursting its lethal effect on MM cells viability and growth. We identified Aurora kinase A (AURKA) inhibitors as top-scoring candidates in both analyses and validated this synergy using functional assays. Finally, we derived a potential model to explain the cooperation between NEAT1 and AURKA in controlling MM biology, providing novel insights into the pathophysiology of this disease.

METHODS

Full details of gymnotic delivery of gapmeRs, cell viability assessment, live cell imaging, cell cycle and drug synergy analyses, reverse transcription and quantitative PCR, western blot, immunofluorescence, DEGs, CoMMpass and survival analyses are provided in supplementary methods.

MM Cell Lines and Drugs

AMO-1, NCI-H929, and MM1.S were purchased from DSMZ. AMO-1 SAM gSCR and AMO-1 SAM gN#8 cell lines were obtained as previously described[20]. Human MM cell lines (HMLC) were immediately expanded and frozen upon arrival and used from the original stock within 6 months. HMCL were cultured in RPMI-1640 medium (Gibco®, Life Technologies, Carlsbad, CA, USA) supplemented with 10% fetal bovine serum, 1% penicillin-streptomycin (Euroclone, Milan, Italy) at 37°C in 5% CO_2 atmosphere. All cell lines were routinely tested for Mycoplasma contamination using the Lonza Mycoalert Mycoplasma Detection Kit (Euroclone, Milan, Italy). Re-authentication by SNP profiling at Multiplexion GmbH (Heidelberg, Germany) was performed for AMO-1, NCI-H929, MM1.S cell lines in 2023. Alisertib and AURKAi-I were purchased from Selleckem and resuspended in DMSO at a stock concentration of 10 mM.

Highthroughput screening

A primary screening using a library of 320 small-molecule inhibitors targeting 123 key proteins was conducted on AMO-1 cells, as previously described[21-22]. The cells were treated with gapmeR NEAT1 (gNEAT1 5 μM) or a control at day 0 and after 24 hours were exposed to the inhibitor library at three different concentrations or to DMSO (vehicle). Cell viability was measured CellTiter-Glo (Promega) luminescence assay at day 0 (d=0) and three days after treatment (d=3), in duplicate. Full details are reported in supplementary methods.

RNA-sequencing

RNA seq libraries were obtained starting from 500 ng of total RNA following the TruSeq Stranded Total RNA (San Diego, CA, USA) protocol. Sequencing was performed with NextSeq 500 sequencer (Illumina) using a 2 × 150 high-output flow cell with 8 samples/run.). Details are described in supplementary methods.

Ethical approval

All patients' data are derived from the publicly available CoMMpass dataset.

RESULTS

AURKA inhibition mimics NEAT1 KD transcriptomic signature.

To identify small compounds that could potentiate the effect of NEAT1 inhibition in MM, we developed an integrated combinatorial strategy (**Figure 1A**).

First, we used a computational approach to select drugs whose activity could recapitulate the transcriptional perturbations induced by NEAT1 inhibition in MM cells. To this end, we performed bulk RNA-sequencing in NEAT1 KD AMO-1 cell line and the relative control. NEAT1 KD was obtained using LNA-GapmeR (gNEAT1), as previously described[19] (**Suppl. figure S.1**). Differential analysis showed that NEAT1 KD strongly affected the gene expression program in MM cells. A total of 1710 genes resulted significantly deregulated (FDR $\leq$ 0.05) in NEAT1 silenced AMO-1 cells as compared with control cells (**Figure 1B**). Of these, 753 genes (44%) were downregulated, and 957 genes (56%) were upregulated upon NEAT1 KD (**Figure 1 C**).

We used this list to query the Connectivity Map (CMap) database, searching for compounds that could mimic the transcriptional perturbation caused by NEAT1 silencing. We identified 66 small molecules as significantly associated with NEAT1 transcriptomic profiles, including CDKi, MTORi, and AURKi.

Of note, the AURKA inhibitor Alisertib, identified among the top-scoring drugs, has been used clinically in combination with proteasome inhibitors in treatment of MM patients[23] (**Figures 1D-E**).

High-throughput drug screening identifies AURKA inhibitors synergizing with NEAT1 inhibition in AMO-1 cell line.

To identify drugs that could potentiate the anti-tumor effects of NEAT1 inhibition in MM cells and to support our computational analyses, we conducted a functional high-throughput screening using a library of 320 small-molecule inhibitors covering 123 pivotal signaling targets. **Supplementary Table 1** lists the compounds included in the screening. **Figure 2A** illustrates the experimental timeline. Briefly, AMO-1 cells were exposed to the drugs at three different concentrations (10 μM, 1 μM, or 100 nM) in the presence or absence of previous NEAT1 silencing and were evaluated at day 0 and 72 h post-treatment, using an ATP-based luminescent metabolic assay (Cell TiterGlo). The combination effect assessed by excess over Bliss (EOB) score with an arbitrary cut-off of EOB>0.2 defined 35 synergistic candidates, including four Aurora kinase inhibitors (**Figures 2B-C**), A subsequent independent validation in AMO-1 cells measuring both metabolic activity and apoptosis by tetrametylrodamine methyl ester (TMRM) staining confirmed AURKA inhibitors Alisertib (ALS) and Aurora A inhibitor I (AURKAi-I) among the most effective drugs (**Figure 2D**), consistent with the results of the *in-silico* predictions.

Aurora kinase inhibitors increase the cytostatic effect of NEAT1 inhibition in MM cells.

To explore the potential synergy between NEAT1 and AURKA inhibition, we performed an in-depth validation. IC_{50} for Alisertib and Aurora kinase A inhibitor- I was assessed in three different MM cell lines (AMO-1, NCI-H929, and MM1.S). All three cellular models showed a robust and consistent sensitivity to both drugs with IC_{50} values in the range of nM for Alisertib and of μM for AURKAi-I (**Supplementary table 2**). NEAT1 silencing was effective in all three cell models tested (**Suppl. figure S.1**)

Due to the role of AURKA in promoting mitosis, we evaluated the effect of the drugs on the cell cycle profile in the three MM cell lines, through flow cytometry (**Figures 3A-B** and **Suppl. Figures S.2A-B**). As expected, the drugs induced a significant increase in the percentage of cells in G2/M supported by a reduction of pAURKA/AURKA ratio (**Figure 3C**) and, as already described, an increase of PLK1 and CyB1[24], (**Figure 3D**) confirming the proper on-target effects in our system.

To assess the level of synergism between NEAT1 and AURKA inhibition, we calculated the synergy score based on cell proliferation. Two different sublethal concentrations of anti-NEAT1 oligos and three different drug concentrations (corresponding to IC_{20}, IC_{50} and IC_{70}) were used

(**Figures 4A-B**). The combination matrix showed a global moderate synergism between NEAT1 inhibition and both AURKA inhibitors in all three cell models tested (**Suppl. Figure S.3A-B**).
To corroborate these data, we monitored the effect of the combination treatment on cell proliferation over time, using a sublethal concentration of both targeting agents. **Figures 5A-C** show the proliferation curves obtained in these experiments. In all three MM cell models, the combination of NEAT1 KD and Alisertib displayed a major effect compared to the single agents alone. Similarly, AURKAi-I used in combination with NEAT1 KD improved the proliferation inhibition in AMO-1 and NCI-H929 but not in MM1.S.

NEAT1 transactivation reduces the effect of AURKA inhibition on MM cell proliferation.

Given the synergy observed between NEAT1 and AURKA inhibition in MM cells, we aimed to assess whether NEAT1 overexpression could rescue the cell growth inhibition caused by AURKA inhibitors. Of note, we recently showed that a high level of NEAT1 expression in MM cells provides a pro-survival advantage upon cellular stressor stimuli[20]. To this end, we used an AMO-1 cell line engineered with CRISPRa exploiting the SAM system, to constitutively transactivate NEAT1[20].
As already reported by us, a 2-fold increase of NEAT1 expression in transactivated cells, namely AMO-1 SAM gN#8 cells, as compared to the scramble condition, namely AMO-1 SAM gSCR was observed (**Suppl. Figure S.4**). Of note, transactivation of NEAT1 determined an increased resistance to AURKA inhibitors as shown by the higher value of IC_{50} observed in NEAT1 overexpressing cells as compared to the scramble. (**Figures 6A-B.)** Evaluation of the number of cells 72 hours after treatment showed that NEAT1 transactivation exerted a significant protective effect on MM cell viability at all doses of drugs tested (**Figure 6C**).
This evidence is in line with the reported role of NEAT1 in promoting drug resistance[19] and supports the hypothesis of a potential interplay between AURKA and NEAT1 in sustaining MM cell growth.

NEAT1 controls AURKA activity through TPX2 transcriptional modulation.

We performed IF staining by using α-tubulin antibodies to monitor the biological effects of NEAT1 KD on mitosis in NCI-H929 and AMO-1 cells treated with Alisertib.

As already reported[25], we confirmed that Alisertib administration impaired the proper bipolar mitotic spindle formation by causing abnormal and unfunctional structures (**Figure 7A panel ii)**. Interestingly, NEAT1 inhibition induces a prominent reorganization of microtubules (MTs) within the cells with evident local alterations in mitotic spindle orientation (**Figure 7A panel i**). Noticeably, NEAT1 KD in Alisertib treated cells resulted in a dramatic increase of spindle abnormalities, that worsened the effect of the drug alone. In particular, we observed a marked increase in the number of mono-polar and/or multi-polar spindles, as well as the presence of spindles with disorganized MTs (**Figure 7A panel iii, Figure 7B)**. These morphological alterations are indicative of a defective division mechanism, in line with the observed proliferation impairment. Besides, these data indicate a previously underscored interplay between NEAT1 and AURKA in MM cells.

This hypothesis was further confirmed by the analysis of the RNA-seq data obtained in AMO-1 upon NEAT1 silencing (**Figure 1B**). Gene Ontology (GO) analysis of the genes downregulated upon NEAT1 KD highlighted several relevant biological processes affected by this lncRNA. In particular, microtubular cytoskeleton and mitotic spindle organization upon cell division scored among the top ten enriched pathways in this analysis (**Figure 7C**). Several genes involved in microtubular organization during mitosis were observed to be significantly downregulated upon NEAT1 KD in AMO-1 cells (**Supplementary table 3).** Most of these genes were also validated through qRT-PCR in both AMO-1 and NCI-H929 cell lines **(Suppl. figures S.5A-B**). Furthermore, we took advantage from our gene expression profiling data previously obtained in NEAT1 KD NCI-H929 cells[19] to perform GO analysis. The results of this analysis revealed the same enriched biological processes also in NCI-H929 cells upon NEAT1 silencing (**Suppl. figure S.6**).

Among these genes, we identified TPX2, which is an allosteric regulator of AURKA and serves to position AURKA at the level of the mitotic spindle during cell division[26,27] (**Figure 7D**). We confirmed that upon NEAT1 KD, TPX2 is downregulated both at the transcript and protein level in AMO-1 and NCI-H929 cells (**Figure 7E**). Besides, NEAT1 transactivation in AMO-1 cells resulted in a significant trend toward upregulation of TPX2 transcript and protein confirming a positive regulation of NEAT1 on this gene (**Figure 7F**). NEAT1-mediated perturbation of genes, like TPX2, involved in the control of AURKA activity could destabilize further cell division AURKA inhibitors administration, thus explaining the combinatorial effect observed in drug screening.

AURKA and NEAT1 expressions stratify survival in MM patients.

We took advantage of the publicly available CoMMpass dataset to explore the association of AURKA expression with genetic and clinical features of MM patients. To assess AURKA

expression profiles in relation to major molecular aberrations in MM, we investigated 660 MM patients of the CoMMpass cohort for which expression, Non-Synonymous (NS) somatic mutations, and Copy Number Alterations (CNAs) data were available (**Supplementary methods and Supplementary table 4**). Significantly higher AURKA expression levels were observed in MM patients carrying markers of highly aggressive disease as 1q gain/amp, 1p loss, 17p deletions, TP53 alterations, MAF and MYC translocations, and 13q deletion, whereas lower expression levels were evidenced in hyperdiploid (HD) cases (**Suppl. Figure S.7)**. No significant differences in AURKA expression levels were observed in relation to t(11;14) and t(4;14) translocations, or the occurrence of NS somatic mutations in RAS/BRAF, TRAF3, DIS3, or FAM46C genes (data not shown). We investigated the clinical impact of AURKA starting from a dataset of 761 patients for whom survival data was available, focusing on those with low (first quartile) and high (fourth quartile) expression of AURKA. Survival curve analysis showed that AURKA expression was associated with both reduced progression-free survival (PFS) and overall survival (OS) probability (**Suppl. Figures S.8A-B**).

To verify if high AURKA expression levels may represent an independent variable in predicting OS and PFS, we tested high AURKA expression condition and other main molecular or clinical features by Cox regression univariate analysis in 489 MM samples for which all information were available.

Concerning OS, a significantly higher risk of death was observed for cases with higher AURKA expression level (Hazard Ratio, HR=1.54, 95% CI 1.11-2.13, BH adj. p-value=0.030); with regards to PFS, higher AURKA expression level was associated with a significantly higher risk of disease progression (Hazard Ratio, HR=1.57, 95% CI 1.23-2.01, BH adj. p-value=0.0016) (**Supplementary table 5A-B**). Interestingly, when all significant variables were tested in multivariate analysis, we observed that AURKA expression retained its independent prognostic impact on PFS, but not in OS (**Suppl Figures S.9A-B**).

Finally, we evaluated whether AURKA and NEAT1 expression level when considered together, could impact patient's clinical outcome. Despite the finding that NEAT1 expression levels alone do not have a significant impact on patients' survival[13], patients having both high AURKA and NEAT1 expression levels displayed the worst survival curve (**Suppl. Figure S.10)**.

DISCUSSION

Despite the significant improvement in the treatment opportunities observed over the past years, most MM patients suffer from relapse and frequently develop highly aggressive disease, experiencing drug resistance to almost all currently available therapeutic options[28,29]. De-regulation of non-coding transcripts contributes to the progression of this disease affecting essential PCs biological processes[8]. We previously described that MM patients frequently show altered expression lncRNAs, which contribute to tumor progression[30]. Among them, we showed that the lncRNA NEAT1 is crucial in promoting the survival of MM cells and enhancing their resistance to stress stimuli[13]. NEAT1 represents the essential architectural structure of nuclear PSs and is involved in several type of cancers. Besides having a role in transcription regulation, this lncRNA has been described to modulate the expression of genes which are fundamental for the subsistence of cancer cell increasing their ability to withstand treatments[31]. We previously demonstrated that NEAT1 silencing reduces MM cells viability by modulating several genome-associated processes. In particular, we observed that NEAT1 is essential for a proficient activity of the homologous recombination (HR) DNA repair process and that its downregulation caused increased genomic damage[19]. Furthermore, we showed that NEAT1 is essential for the maintenance of the genome integrity that controls through at least two separate mechanisms. On one side, NEAT1 promotes paraspeckles assembly by sustaining the stabilization of essential PSs proteins as NONO, SFPQ and FUS. On the other hand, NEAT1 exercises a tight regulation on DNA damage response by modulating the activation of the molecular axis involving ATM, DNA-PKs kinases and their direct targets pRPA32 and pCHK2[20]. Taken together this evidence supports the rational that MM patients with high genomic instability and harboring higher NEAT1 expression levels could benefit from NEAT1 inhibition. For this reason, NEAT1 is currently regarded as an attractive candidate for therapeutic intervention in MM, prompting the need to develop strategic approaches to counteract its pro-tumoral function. Currently, therapeutic modalities targeting lncRNAs in cancer are under investigation in most *in vivo* models[32]. Encouraging results have been obtained after the implementation of delivery systems for antisense oligonucleotides and antagomirs that can be conjugated with cholesterol or delivered with lipid nanoparticles and liposomes to improve the intracellular affinity for target specific lncRNAs[33].

Despite the advances in targeting lncRNAs in human diseases, it is currently challenging to find a robust strategy that counteracts their action in RNA-based therapies in clinical practice. Given the complexity of targeting RNA molecules, approaches such as the one developed in this work may be of relevance to identify combinations able to burst the effect of specific lncRNAs antisense oligonucleotides, as well as alternative strategies that mimic the transcript inhibition. Within this framework, we developed an integrated computational and functional approach aimed at identifying

drug-based strategies that could potentiate NEAT1 inhibition in impairing MM growth and survival. Two separate strategies were employed. The first was based on the transcriptional alterations induced in MM cells by NEAT1 silencing. The NEAT1 KD-associated gene expression profile was used to search for compounds that could recapitulate the NEAT1 KD transcriptional phenotype, by using a computational strategy. The second was based on the functional high-throughput screening of over 300 small compounds, searching for molecules that could amplify the cytostatic effect of NEAT1 KD on MM cells growth. Both these very different approaches converged on identifying for the first time AURKA inhibitors as a promising cooperating agent for NEAT1 inhibition. AURKA has been already implicated in the progression of MM by regulating the activation of autophagy which represents one of the main causes of drug resistance in MM[34-37]. Indeed, AURKA inhibitors were tested in clinical trials in combination with Bortezomib in relapsed MM confirming that targeting AURKA can potentially overcome the issue of therapy resistance likely, restraining the activation of autophagy when the proteasome is impaired[23].

AURKA is a central serine/threonine kinase for regulating the cell cycle and promoting mitosis, participating in the correct maintenance of the genome information. In mitotic cells, the phosphorylation at Tyr288 promotes the activity of AURKA that localizes at centrosomes to control their maturation and at the mitotic spindle to modulate MT dynamics and chromosomes segregation[38]. Furthermore, AURKA full activation requires the interaction with allosteric regulators, which favors its proper activity during mitosis[39,40]. Due to its central role in cell cycle regulation, AURKA is considered as a pan-essential gene for cancer cells that need to maintain high-speed cell proliferation[41]. For this reason, several AURKA inhibitors have been developed and used in different clinical settings. In our drug screening, 4 different compounds (over 20% of the total drugs identified) targeting this protein were identified. Of these, we fully validated two distinct compounds, Alisertib and Aurora A inhibitor-I by using three different cell lines. Both drugs target the active loop of AURKA, in proximity of Tyr288, blocking its catalytic activity. When administered to MM cells, both drugs resulted in a relevant inhibition of cell growth, independently to the used MM cellular model. These effects were maximized upon NEAT1 silencing. Indeed, combination of NEAT1 KD and AURKA inhibition in all three models showed the strongest impairment of cell proliferation supporting and further validating the synergistic action of these agents. Conversely, we also demonstrated that overexpression of NEAT1 reduces the inhibitory effect of AURKA inhibitors on cell proliferation confirming the potential interplay between the mitotic kinase and this lncRNA.

Searching for the molecular basis of this cooperation, we observed that NEAT1 KD deregulated a large set of genes involved in cytoskeleton organization and microtubular assembly during mitosis.

Noticeably, when we looked at the morphology of MM cells under treatment, we observed that the combination of AURKA inhibitors and NEAT1 KD led to severe cytoskeleton abnormalities with the appearance of monopolar and multipolar spindle, abnormal mitotic structure, and incomplete cytokinesis. Coherently, among the genes that were significantly altered upon NEAT1 silencing in MM cells, we observed several genes that partake to these functions and that affect AURKA function directly or indirectly. Of particular interest, we identified TPX2 as NEAT1 target in MM. This gene encodes a microtubule-associated protein that co-localizes at the spindle level during the M-phase. TPX2 acts as an allosteric regulator of AURKA helping its correct positioning at the mitotic spindle and promoting the active conformational state of the protein[25,42,43]. Downregulation of this mediator, as the consequence of NEAT1 silencing, could further compromise the AURKA activity supporting the effect of the drugs. Indeed, it has been already shown that Alisertib also destabilizes the binding selectivity of TPX2 for AURKA[44].

Even if preliminary and requiring further investigations, this evidence points to a new potential nuclear function of NEAT1 in controlling the cytoskeleton dynamics associated with cell division. The potential involvement of NEAT1 on cytoskeleton dynamics was previously suggested in the context of Alzheimer disease, where this lncRNA was shown to modulate microtubules polymerization *in vitro* and *in vivo*. Specifically, NEAT1 KD mediates the depolymerization of microtubules by regulating the FZD3/GSK3β/p-tau pathway, thus exerting a relevant role concerning the etiology of the disease[45]. Furthermore, in hepatocellular carcinoma ROS-stress induction promotes nuclear PSs disassembly and NEAT1 translocation to the cytosol, where it interacts with the kinesin KIF11 enhancing protein degradation and thus contributing to defective spindle formation[46]. Since AURKA is the master regulator of the structural apparatus of mitosis, the observation that NEAT1 controls cytoskeleton during cell division, offers a potential readout of the synergistic effects that we observed by inhibiting both and highlights the existence of a functional interplay between them. However, we cannot exclude that the interaction between these two molecules can occur also at different levels. In particular, the NEAT1 function in keeping genomic stability and orchestrating the DNA damage response could be a relevant issue. Indeed, it has been reported, in ovarian cancer models, that AURKA inhibition unbalances the DNA damage repair system towards the NHEJ error-prone pathway by promoting DNA-PKCs activity. In the meantime, AURKA inhibition impairs the HR mechanism, through the downregulation of PARP, mimicking a BRCAness condition[47].

In line with a previous report, we confirmed that AURKA is an unfavorable prognostic factor for MM patients being negatively associated with OS and PFS[48]. Conversely, NEAT1 alone as previously described, had limited impact on disease progression and patient prognosis[13]. However,

based on the CoMMpass dataset, MM patients that have high AURKA and high NEAT1 display the worst outcome, compared with the other categories, suggesting that high expression of NEAT1 worsens the prognostic effect of AURKA expression, on MM patients.

Even if it is not a direct proof, this observation strongly supports the hypothesis that NEAT1 and AURKA functionally interact in supporting MM growth and progression, and that combinatorial approaches to target both may represent an effective strategy and a new opportunity in the treatment of MM patients.

References

1. Palumbo A, Anderson K. Multiple myeloma. N Engl J Med. 2011;364(11):1046-1060.
2. Siegel RL, Miller KD, Jemal A. Cancer statistics, 2016. CA Cancer J Clin 2016;66(1):7-30.
3. Rajkumar SV. Multiple myeloma: 2020 update on diagnosis, risk□stratification and management. Am J Hematol. 2020;95(5):548-567.
4. Egan JB, Shi CX, Tembe W, et al.Whole-genome sequencing of multiple myeloma from diagnosis to plasma cell leukemia reveals genomic initiating events, evolution, and clonal tides. Blood. 2012;120(5):1060-1066.
5. Quinn JJ, Chang H. Unique features of long non-coding RNA biogenesis and function. Nat Rev Genet. 2016;17(1):47-62.
6. Wang KC, Chang HY. Molecular Mechanisms of Long Noncoding RNAs. Mol Cell. 2011;43(6):904-914.
7. Chi Y, Wang D, Wang J, Yu W, Yang J. Long non-coding RNA in the pathogenesis of cancers. Cells. 2019;8(9):1015.
8. Ronchetti D, Agnelli L, Taiana E, et al. Distinct lncRNA transcriptional fingerprints characterize progressive stages of multiple myeloma. Oncotarget. 2016;7(12):14814-14830.
9. Taiana E, Gallo Cantafio ME, Favasuli VK, et al. Genomic Instability in Multiple Myeloma: A "Non-Coding RNA" Perspective. Cancers (Basel). 2021;28;13(9):2127.
10. Statello L, Guo CJ, Chen LL, Huarte M. Gene regulation by long non-coding RNAs and its biological functions. Nat Rev Mol Cell Biol. 2021;22(2):96-118.
11. Guru SC, Agarwal SK, Manickam P, et al. A transcript map for the 2.8-Mb region containing the multiple endocrine neoplasia type 1 locus. Genome Res. 1997;7(7):725-735.
12. Naganuma T, Nakagawa S, Tanigawa A, Sasaki YF, Goshima N, Hirose T. Alternative 3′□end processing of long noncoding RNA initiates construction of nuclear paraspeckles. EMBO J. 2012;31(20):4020-4034.
13. Taiana E, Ronchetti D, Favasuli V, et al. Long non-coding RNA NEAT1 shows high expression unrelated to molecular features and clinical outcome in multiple myeloma. Haematologica. 2019;104(2):e72-e76.
14. Clemson CM, Hutchinson JN, Sara SA, et al. An architectural role for a nuclear noncoding RNA: NEAT1 RNA is essential for the structure of paraspeckles. Mol Cell. 2009;33(6):717-726.
15. Chen LL, Carmichael GG. Altered nuclear retention of mRNAs containing inverted repeats in human embryonic stem cells: Functional role of a nuclear noncoding RNA. Mol Cell. 2009;35(4):467-478.
16. Hirose T, Virnicchi G, Tanigawa A, et al. NEAT1 long noncoding RNA regulates transcription via protein sequestration within subnuclear bodies. Mol Biol Cell. 2014;25(1):169-183.
17. Jiang L, Shao C, Wu QJ, et al. NEAT1 scaffollds RNA-binding proteins and the Microprocessor to globally enhance pri-miRNA processing. Nat Struct Mol Biol. 2017;24(10):816-824.
18. Li R, Harvey AR, Hodgetts SI, Fox AH. Functional dissection of NEAT1 using genome editing reveals substantial localization of the NEAT1_1 isoform outside paraspeckles. RNA. 2017;23(6):872-881.
19. Taiana E, Favasuli V, Ronchetti D, et al. Long non-coding RNA NEAT1 targeting impairs the DNA repair machinery and triggers anti-tumor activity in multiple myeloma. Leukemia. 2020;34(1):234-244.
20. Taiana E, Bandini C, Favasuli VK, et al. Activation of lncRNA NEAT1 leads to survival advantage of multiple myeloma cells by supporting a positive regulatory loop with DNA repair proteins. Haematologica. 2020;108(1):219-233.
21. Bandini C, Mereu E, Paradzik T, et al. Lysin (K)-specific demethylase 1 inhibition enhances proteasome inhibitor response and overcomes drug resistance in multiple myeloma. Exp Hematol Oncol. 2023;12(1):71.

22. Mereu E, Abbo D, Paradzik T, et al. Euchromatic Histone Lysine Methyltransferase 2 Inhibition Enhances Carfilzomib Sensitivity and Overcomes Drug Resistance in Multiple Myeloma Cell Lines. Cancers (Basel). 2023;15(8):2199.
23. Rosenthal A, Kumar S, Hofmeister C, et al. A Phase Ib Study of the combination of the Aurora Kinase Inhibitor Alisertib (MLN8237) and Bortezomib in Relapsed Multiple Myeloma. Br J Haematol. 2016;174(2):323-325.
24. Metselaar DS, du Chatinier A, Meel MH, et al. AURKA and PLK1 inhibition selectively and synergistically block cell cycle progression in diffuse midline glioma. iScience. 2022;25(6):104398.
25. Fathi AT, Wander SA, Blonquist TM, et al. Phase I study of the aurora A kinase inhibitor alisertib with induction chemotherapy in patients with acute myeloid leukemia. Haematologica. 2017;102(4):719-727.
26. Kufer TA, Silljé HH, Körner R, Gruss OJ, Meraldi P, Nigg EA. TPX2 is required for targeting Aurora-A kinase to the spindle. J Cell Bio. 2022;158(4):617-623.
27. Eyers PA, Erikson E, Chen LG, Maller JL. A novel mechanism for activation of the protein kinase Aurora A. Curr Biol. 2023;13(8):691-697.
28. Yang WC, Lin SF. Mechanisms of Drug Resistance in Relapse and Refractory Multiple Myeloma. Biomed Res Int. 2015;2015:341430.
29. Vo JN, Wu YM, Mishler J, et al. The genetic heterogeneity and drug resistance mechanisms of relapsed refractory multiple myeloma. Nat Commun. 2022;13(1):3750.
30. Ronchetti D, Agnelli L, Pietrelli A, et al. A compendium of long non-coding RNAs transcriptional fingerprint in multiple myeloma. Sci Rep. 2018;8(1):6557.
31. Pistoni M, Rossi T, Donati B, Torricelli F, Polano M, Ciarrocchi A. Long Noncoding RNA NEAT1 Acts as a Molecular Switch for BRD4 Transcriptional Activity and Mediates Repression of BRD4/WDR5 Target GenesTranscriptional Repression via lncRNA NEAT1/BRD4 Interaction. Mol Cancer Res. 2011;19(5):799-811.
32. Ling H, Fabbri M, Calin GA. MicroRNAs and other non-coding RNAs as targets for anticancer drug development. Nat Rev Drug Discov. 2013;12(11):847-865.
33. Roberts TC, Langer R, Wood MJA. Advances in oligonucleotide drug delivery. Nat Rev Drug Discov. 2020;19(10):673-694.
34. Xie Y, Zhu S, Zhong M, et al. Inhibition of Aurora Kinase A Induces Necroptosis in Pancreatic Carcinoma. Gastroenterology. 2017;153(5):1429-1443.
35. Wang P, Gong Y, Guo T, et al. Activation of Aurora A kinase increases YAP stability via blockage of autophagy. Cell Death Dis. 2019;10(6):432.
36. Tang A, Gao K, Chu L, Zhang R, Yang J, Zheng J. Aurora kinases: novel therapy targets in cancers. Oncotarget. 2017;8(14):23937-23954.
37. Murga-Zamalloa C, Inamdar KV, Wilcox RA. The role of aurora A and polo-like kinases in high-risk lymphomas. Blood Adv 2019;3(11):1778-1787.
38. Naso FD, Boi D, Ascanelli C, et al. Nuclear localisation of Aurora-A: its regulation and significance for Aurora-A functions in cancer. Oncogene. 2021;40(23):3917-3928.
39. Garrido G, Vernos I. Non-centrosomal TPX2-Dependent Regulation of the Aurora A Kinase: Functional Implications for Healthy and Pathological Cell Division. Front Oncol. 2016;6:88.
40. Mou PK, Yang EJ, Shi C, Ren G, Tao S, Shim JS. Aurora kinase A, a synthetic lethal target for precision cancer medicine. Exp Mol Med. 2021;53(5):835-847.
41. Hose D, Rème T, Hielscher T, et al. Proliferation is a central independent prognostic factor and target for personalized and risk-adapted treatment in multiple myeloma. Haematologica. 2011;96(1):87-95.
42. Bayliss R, Sardon T, Vernos I, Conti E. Structural basis of Aurora-A activation by TPX2 at the mitotic spindle. Mol Cell. 2003;12(4):851-862.
43. Levinson NM. The multifaceted allosteric regulation of Aurora kinase A. Biochem J. 2018;475(12):2025-2042.

44. Lake EW, Muretta JM, Thompson AR, et al. Quantitative conformational profiling of kinase inhibitors reveals origins of selectivity for Aurora kinase activation states. Proc Natl Acad Sci U S A. 2018;18;115(51):E11894-E11903.
45. Zhao Y, Wang Z, Mao Y, et al. NEAT1 regulates microtubule stabilization via FZD3/GSK3β/P-tau pathway in SH-SY5Y cells and APP/PS1 mice. Aging (Albany NY). 2020;12(22):23233-23250.
46. Chen D, Wang J, Li Y, et al. LncRNA NEAT1 suppresses cellular senescence in hepatocellular carcinoma via KIF11-dependent repression of CDKN2A. Clin Transl Med. 2023;(9):e1418.
47. Do TV, Hirst J, Hyter S, Roby KF, Godwin AK. Aurora A kinase regulates non-homologous end-joining and poly(ADP-ribose) polymerase function in ovarian carcinoma cells. Oncotarget. 2019;8(31):50376-50392.
48. Hose D, Rème T, Meissner T, et al. Inhibition of aurora kinases for tailored risk-adapted treatment of multiple myeloma. Blood. 2009;113(18)4331-4340.

LEGENDS TO FIGURES

Figure 1. AURKA inhibition mimics NEAT1 KD transcriptomic signature. A) Framework overview: computational and functional approaches adopted to identify compounds exerting a synergistic activity with total NEAT1 silencing in MM cells.

B) Volcano plot showing significantly down (green) and up (red) - regulated genes in AMO-1 NEAT1 KD cells compared to scramble condition (lnFC ≤ | 0,7 | padj ≤ 0.05). **C)** Pie chart showing the number of significantly down and up-regulated genes in AMO-1 NEAT1 KD cells compared to scramble condition (lnFC ≤ | 0,7 | padj ≤ 0.05). **D)** Alluvial plot depicting top scoring molecules derived from cMap query, in particular: inhibitors (left), the class of perturbation they belong (middle), and their target genes (right). **E)** Heatmap showing the relative cMap score of the 33 top-scoring candidate compounds with score >90.

Figure 2. **HT drug screening identifies AURKA inhibitors as promising synergistic agents when combined with NEAT1 inhibition. A)** Experimental overview of drugs screening. AMO-1 cells were seeded and silenced for NEAT1 expression (day -1) through gymnotic delivery of LNA-GapmeR (gNEAT1). Cell viability was assessed using ATP assay after 24 hours (day 0) followed by treatment with three different concentrations of compounds. At 96 hours of NEAT1 silencing and 72 hours of compounds treatment (day 3) cells viability was assessed by ATP assay and NEAT1 expression was quantified through qRT-PCR. Combined drug effect was determined by Excess over Bliss (EOB) analysis. **B)** Diagram illustrating the top 35 top candidates (EOB > 0.2) exhibiting synergistic effect when combined with NEAT1 silencing. **C**) Sunburst diagram depicting the category of compounds and the name of the drugs that exert a synergistic activity with NEAT1 KD. **D)** AMO-1 cells viability was evaluated by ATP assay (upper diagram) in duplicate and flow-cytometry (lower diagram) in the presence or absence of gNEAT1. Statistical significance was measured with Student's t test *p < 0.05 **P<0.01 or ***P<0.001.

Figure 3. HMLCs showed a robust sensitivity to AURKA inhibitors. FACS analysis of cell cycle phases distribution after Alisertib (**A**) and AURKAi-I (**B**) treatments (24 hours) in AMO-1, NCI-H929 and MM1.S cells. The histogram chart shows the percentage of cell cycle distribution is represented in the histogram; standard deviation of three replicates is reported, *p < 0.05, **p < 0.01, ***p < 0.001, Student's t test. **C)** WB analyses showing pAURKA and AURKA protein expression after Alisertib (24 hours) and AURKAi-I (6 hours) treatments in AMO-1, NCI-H929 and MM1.S cells. **D)** WB analyses showing CyCB1 and PLK1 cell cycle checkpoints proteins after Alisertib and AURKAi-I treatments (24 hours).

Figure 4. Synergy assessment through the calculation of CI. Histograms depicting raw-data of combination indexes (CI): fraction of viable AMO-1, NCI-H929, and MM1.S cells after four days NEAT1 silencing and three days of treatment with the indicated concentrations of Alisertib (**A**) and AURKAi-I (**B**).

Figure 5. AURKAi increases the cytostatic effect of NEAT1 inhibition in MM overtime.
Live cell imaging analysis: proliferation rate was measured relative to T = 0 h, in AMO-1 (**A**), NCI-H929 (**B**), MM1.S (**C**) MM cell lines with Incucyte S3 Live Cell Analysis (Sartorius). AMO-1, NCI-H929 and MM1.S were silenced for NEAT1 expression with different concentrations of GapmeR and treated with IC_{20} concentration of Alisertib or AURKAi-I. Values are represented as the ratio between the treated sample over the vehicle. The graph shows the mean ± SEM of two independent experiments. Statistical significance was measured with Student's t test *p < 0.05 ***P*<0.01 or ****P*<0.001.

Figure 6. NEAT1 transactivation determines an increased resistance to AURKA inhibitors.
IC_{50} curve of Alisertib and AURKAi-I in AMO-1 SAM cell lines. IC_{50} value was calculated at 72 hours of treatment using the Compusyn software. Fraction of alive cells (%) is provided on vertical axis and log (concentration) [µM] of Alisertib (**A**) and AURKAi-I (**B**) on horizontal axis. **C)** Histogram showing the biological effect obtained in AMO-1 SCR and AMO-1 N#8 SAM treated with Alisertib and AURKAi-I. Values are represented as the ratio between the treated samples over the vehicle. The graph shows the mean ± SEM of two independents biological replicates. Statistical significance was measured with Student's t test *p < 0.05, ***P*<0.01 or ****P*<0.001.

Figure 7. NEAT1 is involved mitotic spindle dynamics by controlling AURKA activity through TPX2 transcriptional modulation. A) Representative images of metaphase spindles. AMO-1 and NCI-H929 cells treated with Vehicle, gNEAT1, Alisertib, Alisertib + gNEAT1. α-Tubulin was stained in green and DAPI was used to stain cell nuclei. Scale bar 20 µm. **B)** Bar plot representing the percentage of mitotic cells with defective spindles in AMO-1 and NCI-H929 treated with Vehicle, gNEAT1, Alisertib, Alisertib + gNEAT1. **C)** Dot plot of the top ten down-regulated significant biological processes (FDR<0.05) obtained in AMO-1 NEAT1 KD cells. **D)** STRING node depicting functional and physical protein –protein interaction among the down-regulated genes related to mitotic spindle and microtubule organization in AMO-1 NEAT1 KD cells. **E**) Quantitative real-time PCR of TPX2 in AMO-1 and NCI-H929 cells silenced for NEAT1 expression (gNEAT1) and in the relative control condition (gSCR), after gapmeRs delivery and WB

analysis of TPX2 protein in AMO-1 and NCI-H929 cells silenced for NEAT1 expression (gNEAT1) and in the relative control condition (gSCR), after gapmeRs delivery (n = 3). **F**) Quantitative real-time PCR of TPX2 in AMO-1 SAM gSCR and AMO-1 SAM gN#8 cells and WB analysis of TPX2 protein in AMO-1 SAM gSCR and AMO-1 SAM gN#8 cells (n = 2).

Figure 1

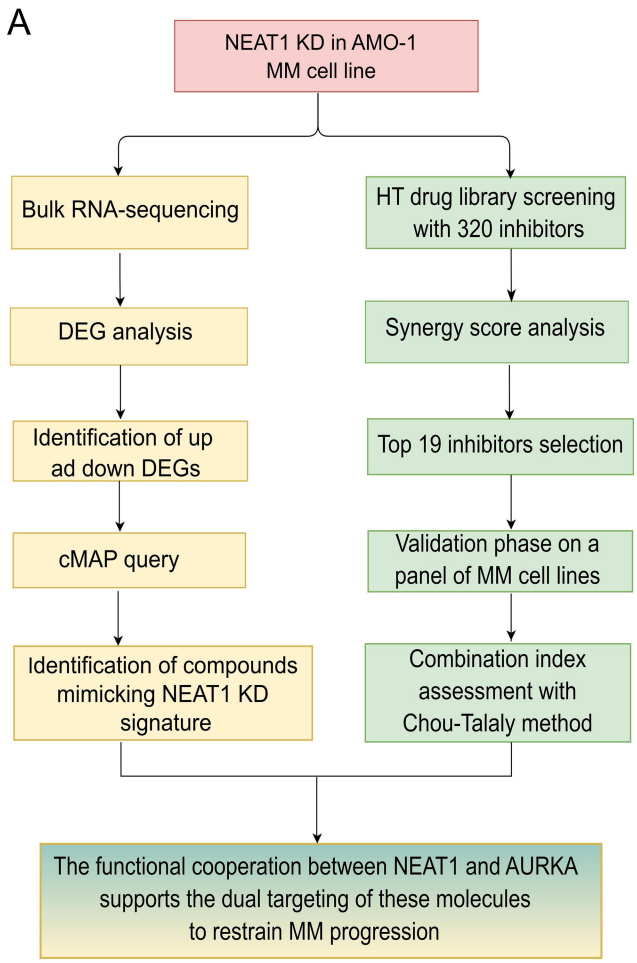
A
NEAT1 KD in AMO-1 MM cell line
Bulk RNA-sequencing
HT drug library screening with 320 inhibitors
DEG analysis
Synergy score analysis
Identification of up ad down DEGs
Top 19 inhibitors selection
cMAP query
Validation phase on a panel of MM cell lines
Identification of compounds mimicking NEAT1 KD signature
Combination index assessment with Chou-Talaly method
The functional cooperation between NEAT1 and AURKA supports the dual targeting of these molecules to restrain MM progression

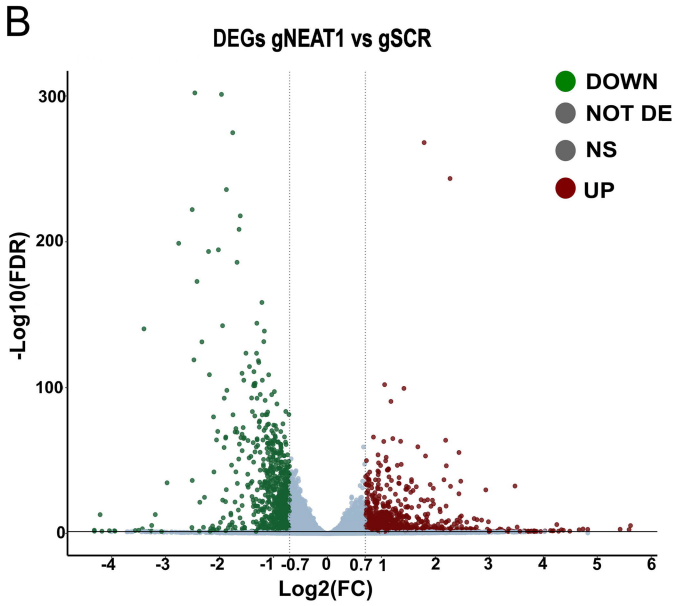
B
DEGs gNEAT1 vs gSCR
DOWN
NOT DE
NS
UP
-Log10(FDR)
Log2(FC)

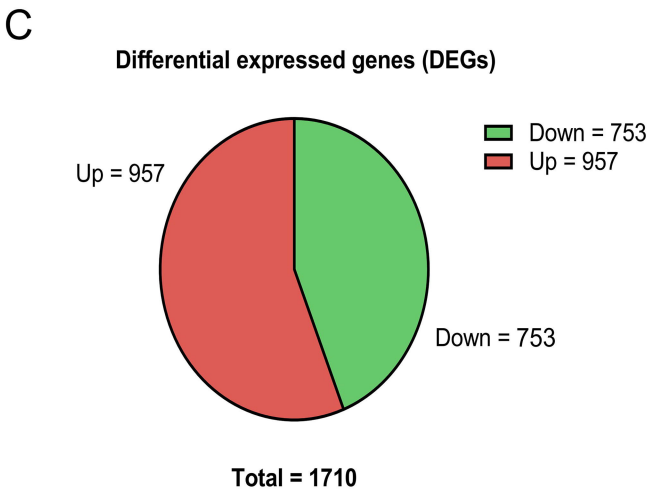
C
Differential expressed genes (DEGs)
Down = 753
Up = 957
Up = 957
Down = 753
Total = 1710

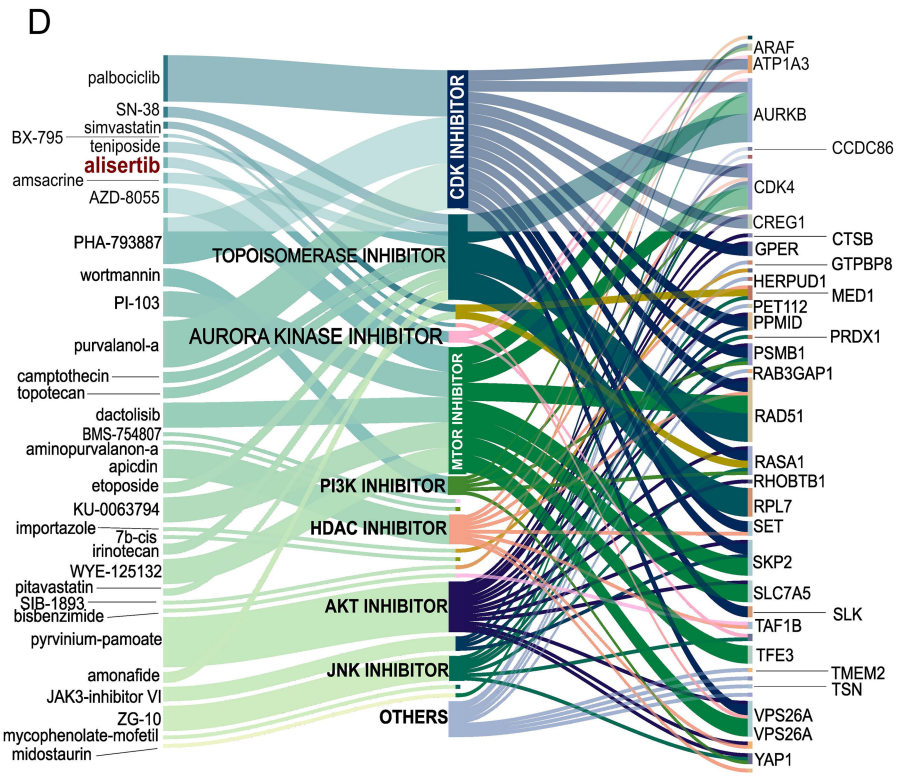
D
palbociclib
SN-38
simvastatin
BX-795
teniposide
alisertib
amsacrine
AZD-8055
PHA-793887
wortmannin
PI-103
purvalanol-a
camptothecin
topotecan
dactolisib
BMS-754807
aminopurvalanon-a
apicdin
etoposide
KU-0063794
importazole
7b-cis irinotecan
WYE-125132
pitavastatin
SIB-1893
bisbenzimide
pyrvinium-pamoate
amonafide
JAK3-inhibitor VI
ZG-10
mycophenolate-mofetil
midostaurin
CDK INHIBITOR
TOPOISOMERASE INHIBITOR
AURORA KINASE INHIBITOR
MTOR INHIBITOR
PI3K INHIBITOR
HDAC INHIBITOR
AKT INHIBITOR
JNK INHIBITOR
OTHERS
ARAF
ATP1A3
AURKB
CCDC86
CDK4
CREG1
CTSB
GPER
GTPBP8
HERPUD1
MED1
PET112
PPMID
PRDX1
PSMB1
RAB3GAP1
RAD51
RASA1
RHOBTB1
RPL7
SET
SKP2
SLC7A5
SLK
TAF1B
TFE3
TMEM2
TSN
VPS26A
VPS26A
YAP1

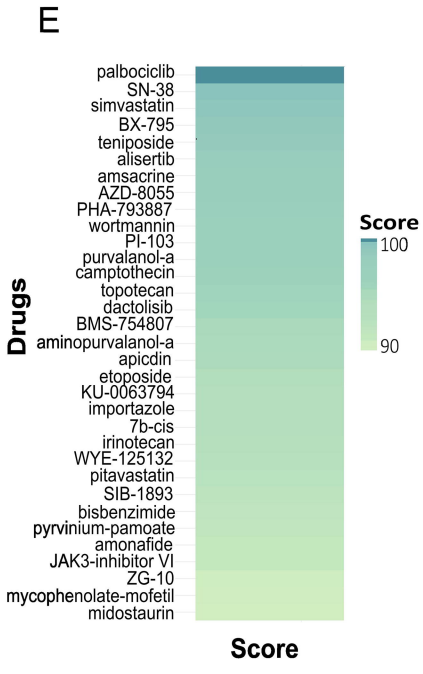
E
palbociclib
SN-38
simvastatin
BX-795
teniposide
alisertib
amsacrine
AZD-8055
PHA-793887
wortmannin
PI-103
purvalanol-a
camptothecin
topotecan
dactolisib
BMS-754807
aminopurvalanol-a
apicdin
etoposide
KU-0063794
importazole
7b-cis irinotecan
WYE-125132
pitavastatin
SIB-1893
bisbenzimide
pyrvinium-pamoate
amonafide
JAK3-inhibitor VI
ZG-10
mycophenolate-mofetil
midostaurin
Drugs
Score
100
90
Score

Figure 2

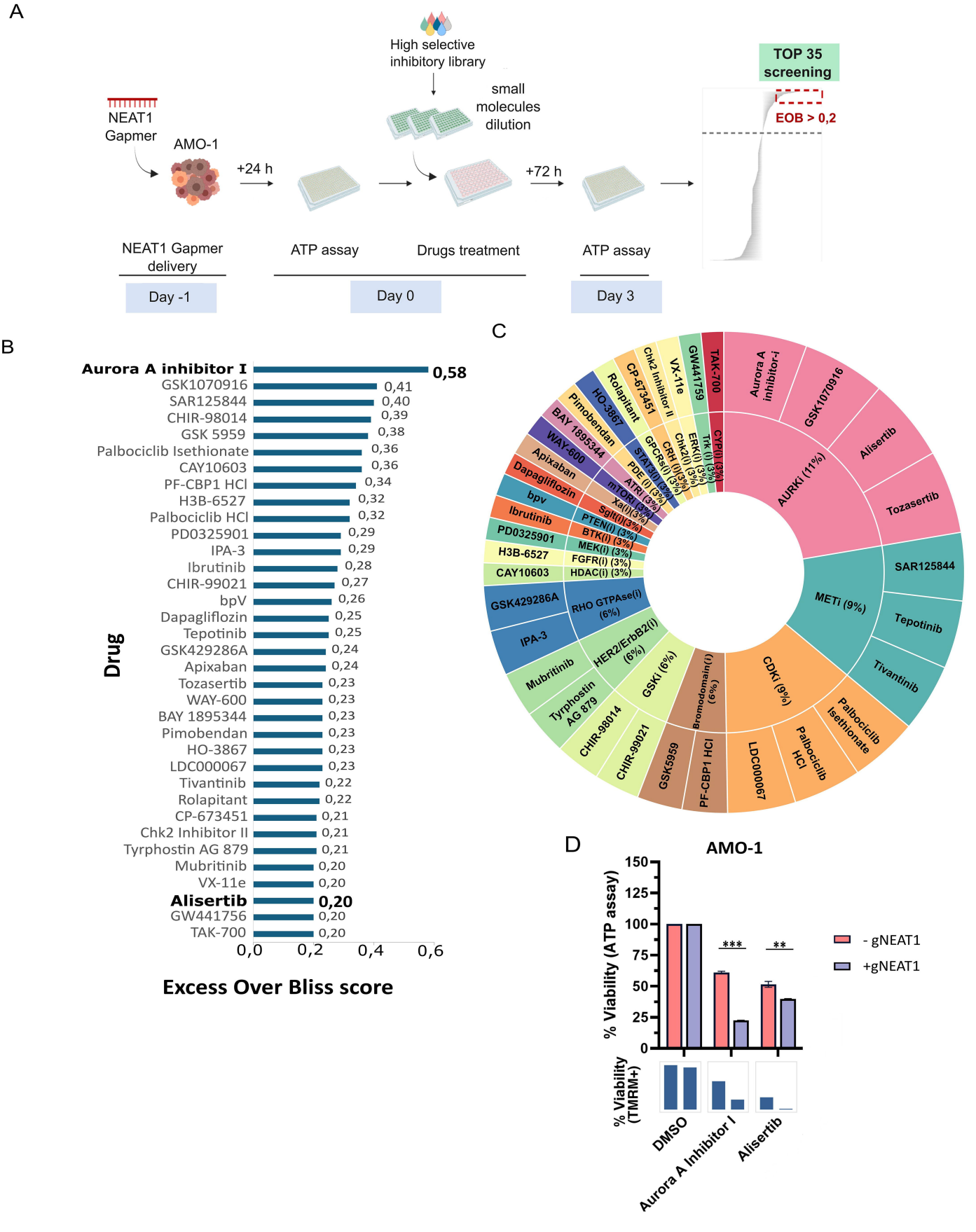
A
High selective inhibitory library
small molecules dilution
TOP 35 screening
EOB > 0,2
NEAT1 Gapmer
AMO-1
+24 h
+72 h
NEAT1 Gapmer delivery
ATP assay
Drugs treatment
ATP assay
Day -1
Day 0
Day 3
B
Aurora A inhibitor I 0,58
GSK1070916 0,41
SAR125844 0,40
CHIR-98014 0,39
GSK 5959 0,38
Palbociclib Isethionate 0,36
CAY10603 0,36
PF-CBP1 HCl 0,34
H3B-6527 0,32
Palbociclib HCl 0,32
PD0325901 0,29
IPA-3 0,29
Ibrutinib 0,28
CHIR-99021 0,27
bpV 0,26
Dapagliflozin 0,25
Tepotinib 0,25
GSK429286A 0,24
Apixaban 0,24
Tozasertib 0,23
WAY-600 0,23
BAY 1895344 0,23
Pimobendan 0,23
HO-3867 0,23
LDC000067 0,23
Tivantinib 0,22
Rolapitant 0,22
CP-673451 0,21
Chk2 Inhibitor II 0,21
Tyrphostin AG 879 0,21
Mubritinib 0,20
VX-11e 0,20
Alisertib 0,20
GW441756 0,20
TAK-700 0,20
Drug
0,0 0,2 0,4 0,6
Excess Over Bliss score
C
Aurora A inhibitor-i
GSK1070916
Alisertib
Tozasertib
AURKi (11%)
SAR125844
Tepotinib
Tivantinib
METi (9%)
Palbociclib Isethionate
Palbociclib HCl
LDC000067
CDKi (9%)
PF-CBP1 HCl
GSK5959
CHIR-99021
CHIR-98014
Tyrphostin AG 879
Mubritinib
GSK1 (6%)
HER2/ErbB2(i) (6%)
Bromodomain(i) (6%)
RHO GTPAse(i) (6%)
IPA-3
GSK429286A
CAY10603
H3B-6527
PD0325901
Ibrutinib
bpv
Dapagliflozin
Apixaban
WAY-600
BAY 1895344
Pimobendan
HO-3867
Rolapitant
CP-673451
Chk2 Inhibitor II
VX-11e
GW441759
TAK-700
CYPB(i) (3%)
Trk (i) (3%)
ERK(i) (3%)
Chk2(i) (3%)
CRH (i)(3%)
GPCRs(i) (3%)
STAT3(i) (3%)
PDE (i) (3%)
ATR(i) (3%)
mTOR(i) (3%)
Xa(i)(3%)
Sglt(i)(3%)
PTEN(i) (3%)
BTK(i) (3%)
MEK(i) (3%)
FGFR(i) (3%)
HDAC(i) (3%)
D
AMO-1
% Viability (ATP assay)
150
125
100
75
50
25
0
***
**
- gNEAT1
+gNEAT1
% Viability (TMRM+)
DMSO
Aurora A Inhibitor I
Alisertib

Figure 3

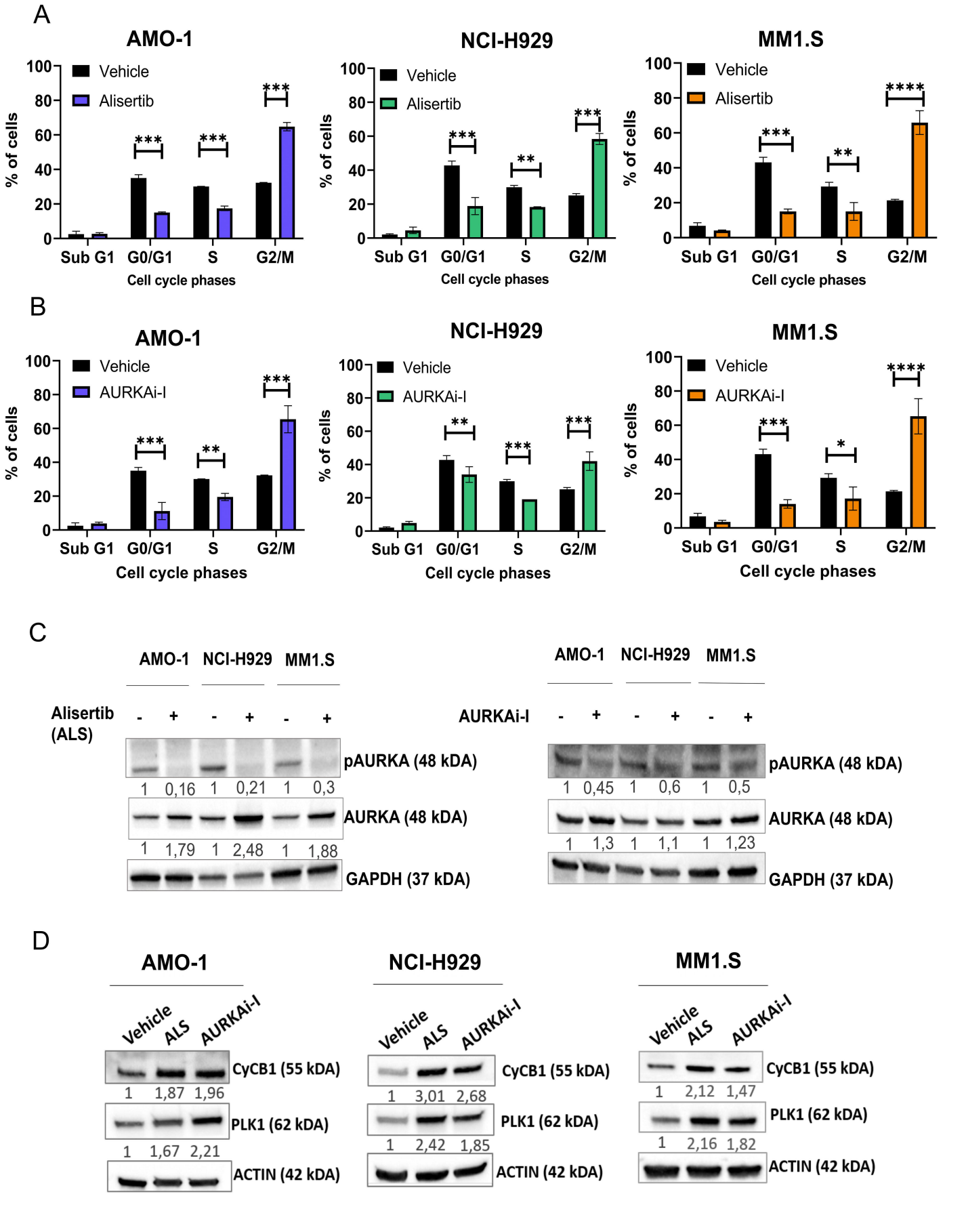
A
AMO-1
NCI-H929
MM1.S
Vehicle
Alisertib
% of cells
Sub G1
G0/G1
S
G2/M
Cell cycle phases
B
AMO-1
NCI-H929
MM1.S
Vehicle
AURKAi-I
% of cells
Sub G1
G0/G1
S
G2/M
Cell cycle phases
C
AMO-1
NCI-H929
MM1.S
Alisertib (ALS)
pAURKA (48 kDA)
1 0,16 1 0,21 1 0,3
AURKA (48 kDA)
1 1,79 1 2,48 1 1,88
GAPDH (37 kDA)
AURKAi-I
pAURKA (48 kDA)
1 0,45 1 0,6 1 0,5
AURKA (48 kDA)
1 1,3 1 1,1 1 1,23
GAPDH (37 kDA)
D
AMO-1
NCI-H929
MM1.S
Vehicle
ALS
AURKAi-I
CyCB1 (55 kDA)
1 1,87 1,96
PLK1 (62 kDA)
1 1,67 2,21
ACTIN (42 kDA)
1 3,01 2,68
1 2,42 1,85
1 2,12 1,47
1 2,16 1,82

Figure 4

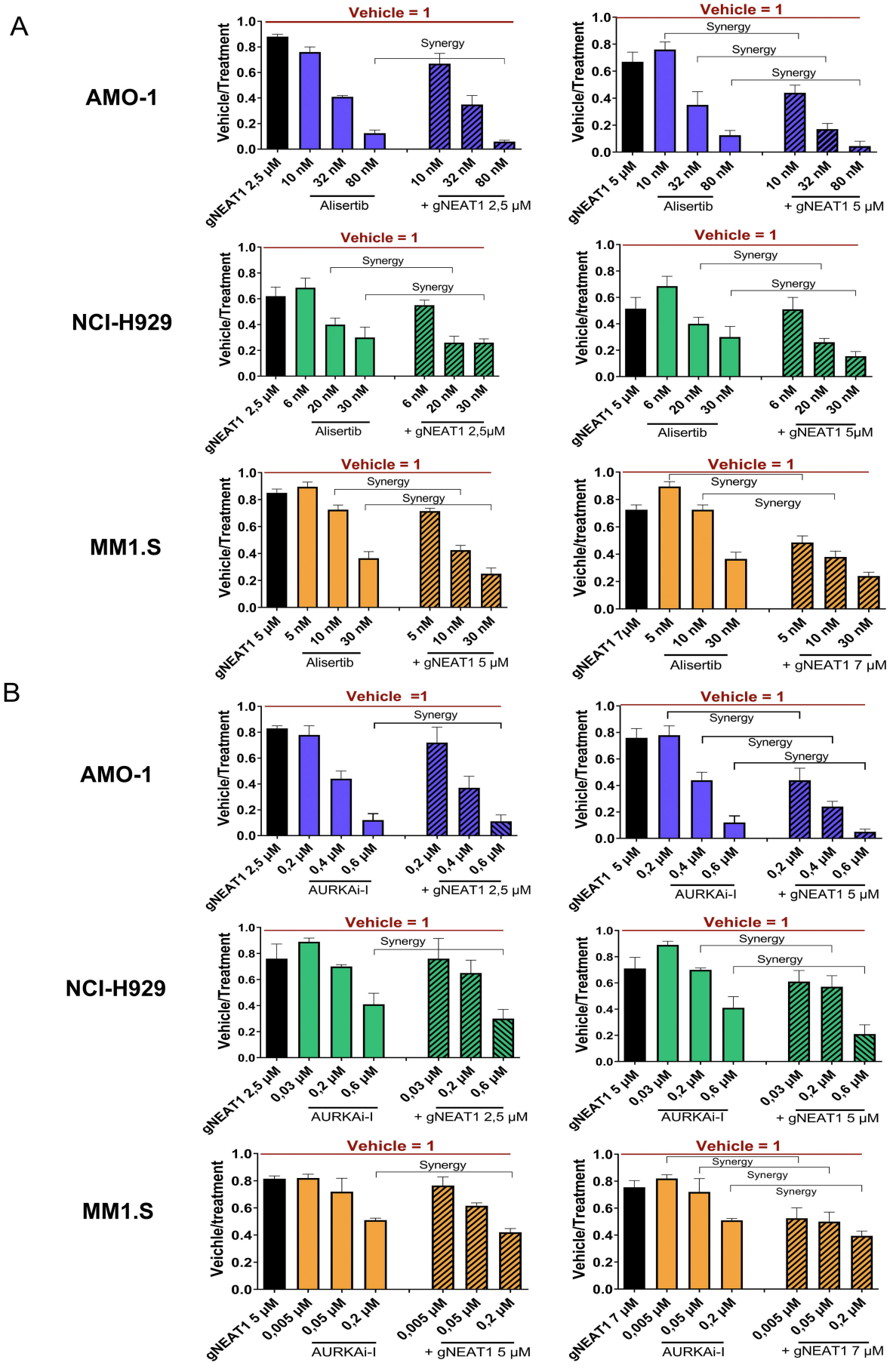
A
AMO-1
NCI-H929
MM1.S
B
AMO-1
NCI-H929
MM1.S
Vehicle = 1
Vehicle =1
Synergy
Vehicle/Treatment
Vehicle/treatment
Veichle/treatment
gNEAT1 2,5 µM
gNEAT1 5 µM
gNEAT1 7µM
10 nM
32 nM
80 nM
6 nM
20 nM
30 nM
5 nM
10 nM
30 nM
0,2 µM
0,4 µM
0,6 µM
0,03 µM
0,005 µM
0,05 µM
0,2 µM
Alisertib
AURKAi-I
+ gNEAT1 2,5 µM
+ gNEAT1 5 µM
+ gNEAT1 7 µM

Figure 5

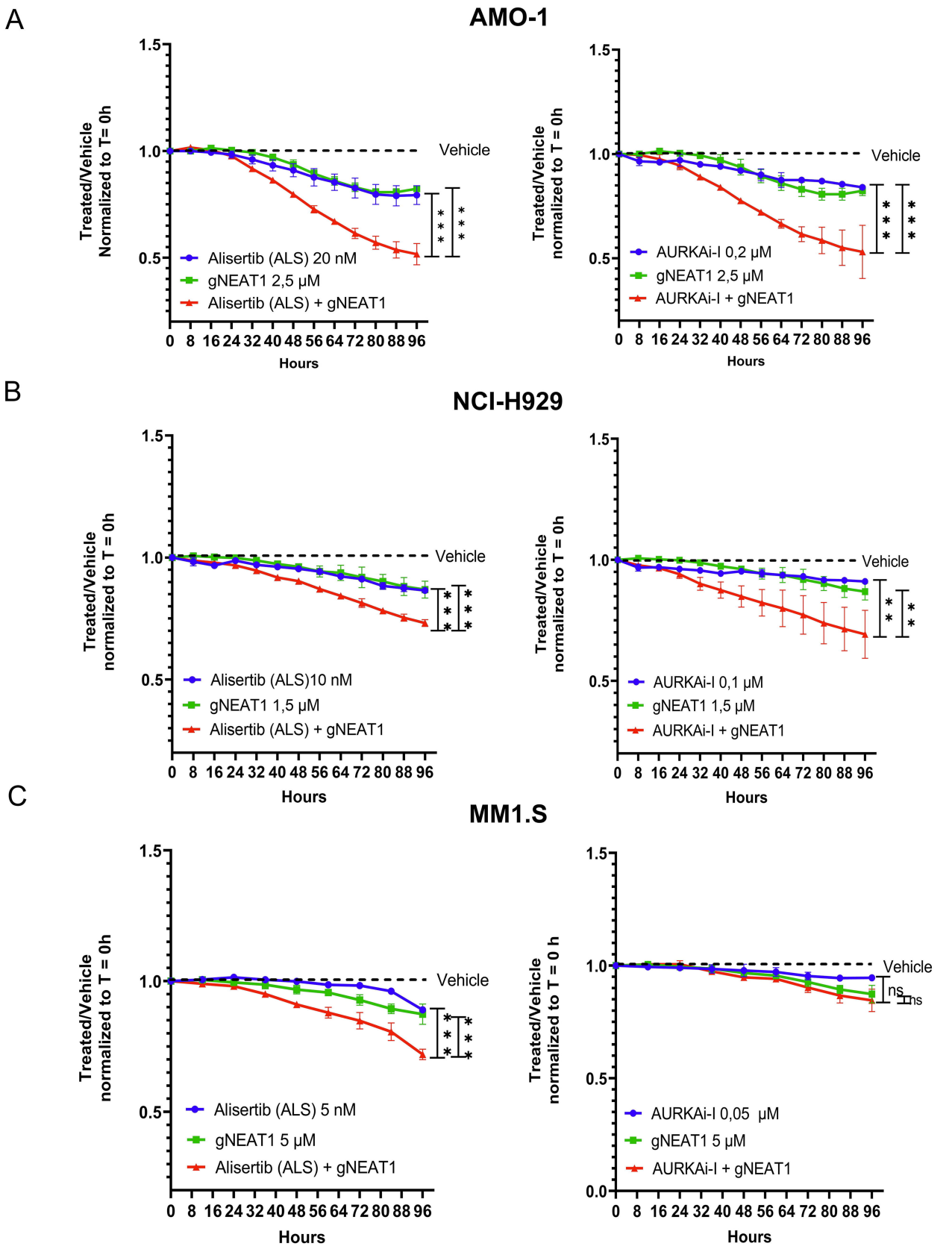
A
AMO-1
Treated/Vehicle Normalized to T= 0h
Vehicle
Alisertib (ALS) 20 nM
gNEAT1 2,5 µM
Alisertib (ALS) + gNEAT1
Hours
Treated/Vehicle normalized to T = 0h
AURKAi-I 0,2 µM
gNEAT1 2,5 µM
AURKAi-I + gNEAT1
B
NCI-H929
Alisertib (ALS)10 nM
gNEAT1 1,5 µM
AURKAi-I 0,1 µM
C
MM1.S
Alisertib (ALS) 5 nM
gNEAT1 5 µM
AURKAi-I 0,05 µM
Treated/Vehicle normalized to T = 0 h
ns

Figure 6

A

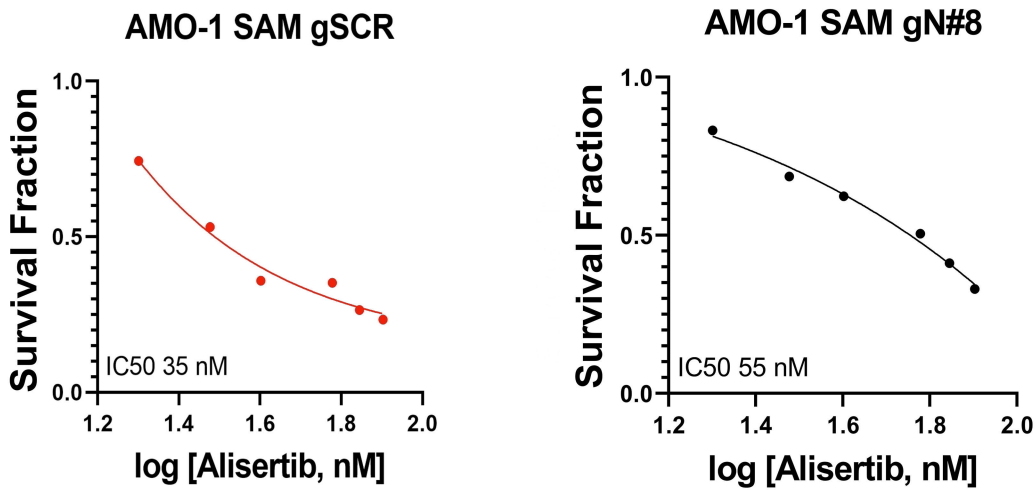
AMO-1 SAM gSCR
Survival Fraction
1.0
0.5
0.0
IC50 35 nM
1.2
1.4
1.6
1.8
2.0
log [Alisertib, nM]
AMO-1 SAM gN#8
Survival Fraction
1.0
0.5
0.0
IC50 55 nM
1.2
1.4
1.6
1.8
2.0
log [Alisertib, nM]

B

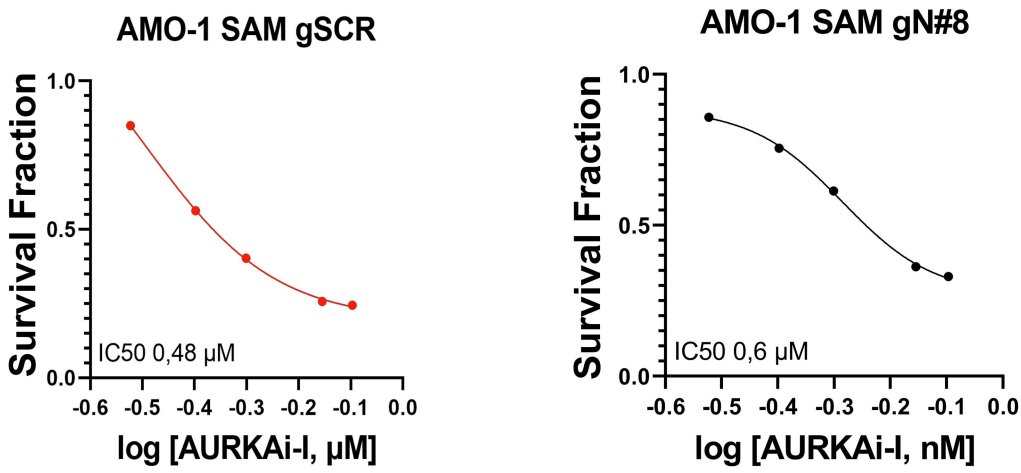
AMO-1 SAM gSCR
Survival Fraction
1.0
0.5
0.0
IC50 0,48 µM
-0.6
-0.5
-0.4
-0.3
-0.2
-0.1
0.0
log [AURKAi-l, µM]
AMO-1 SAM gN#8
Survival Fraction
1.0
0.5
0.0
IC50 0,6 µM
-0.6
-0.5
-0.4
-0.3
-0.2
-0.1
0.0
log [AURKAi-l, nM]

C

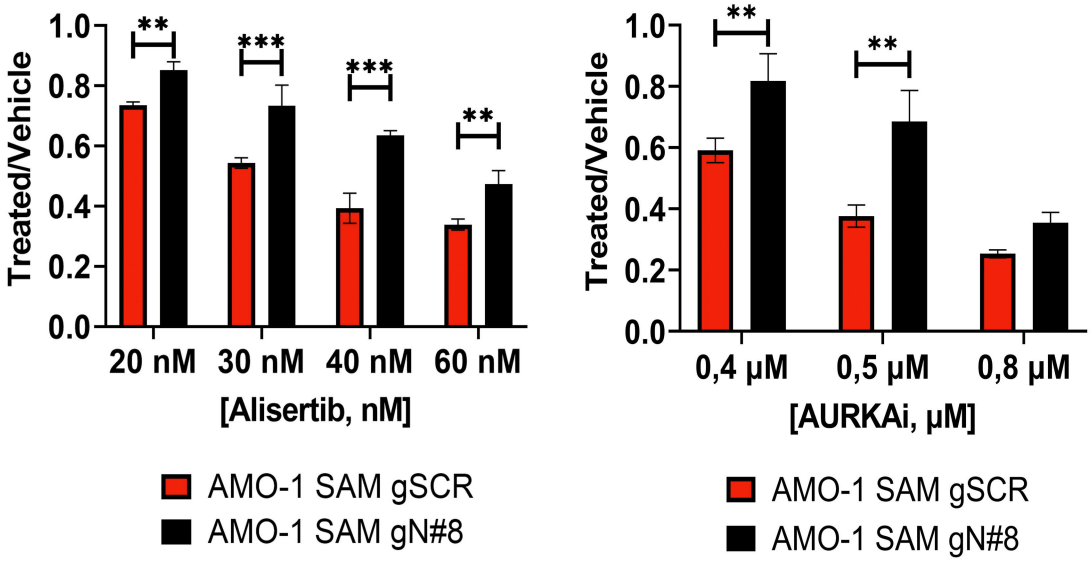
Treated/Vehicle
1.0
0.8
0.6
0.4
0.2
0.0
**
***
***
**
20 nM
30 nM
40 nM
60 nM
[Alisertib, nM]
AMO-1 SAM gSCR
AMO-1 SAM gN#8
Treated/Vehicle
1.0
0.8
0.6
0.4
0.2
0.0
**
**
0,4 µM
0,5 µM
0,8 µM
[AURKAi, µM]
AMO-1 SAM gSCR
AMO-1 SAM gN#8

Figure 7

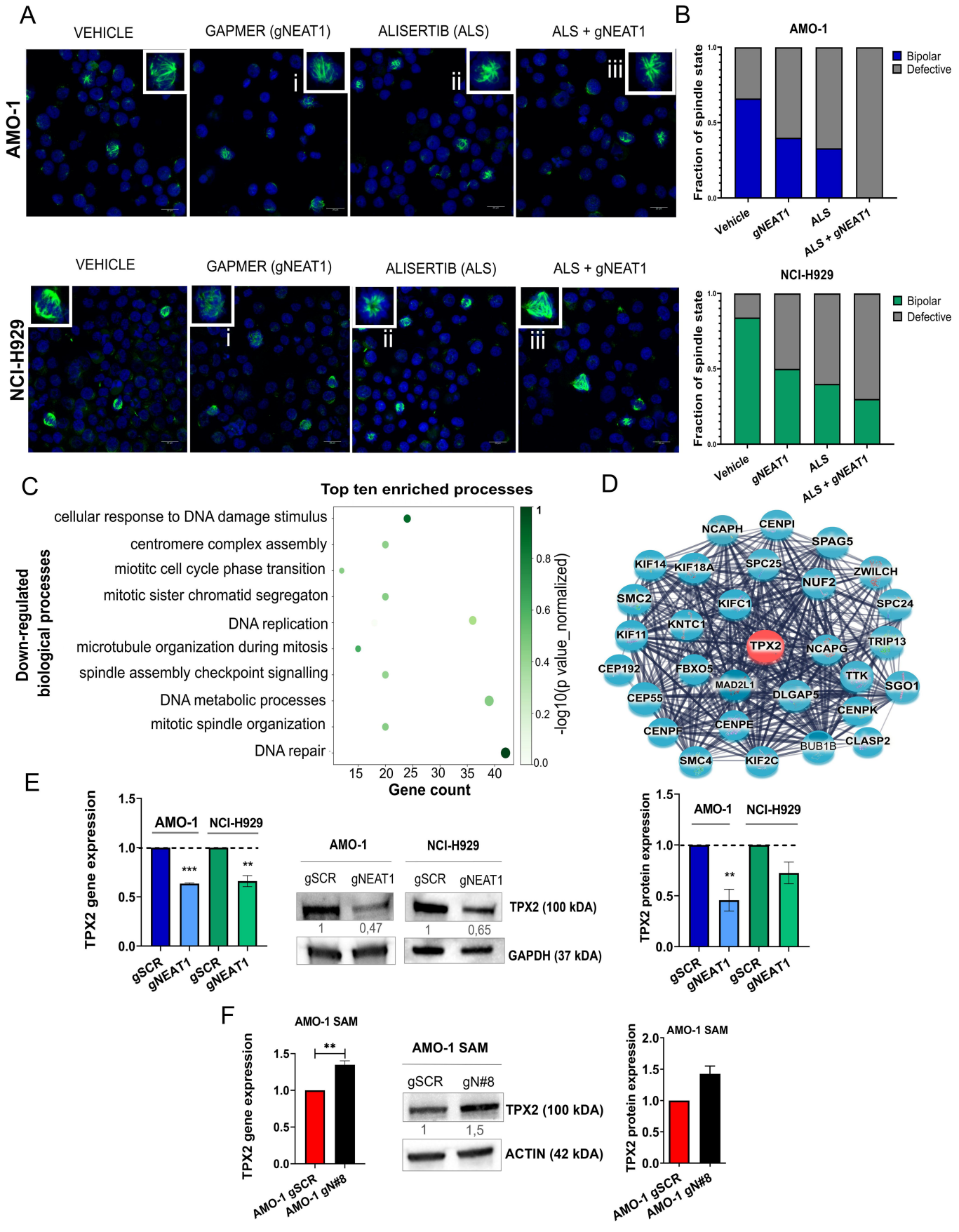
A
VEHICLE
GAPMER (gNEAT1)
ALISERTIB (ALS)
ALS + gNEAT1
AMO-1
NCI-H929
i
ii
iii
B
AMO-1
NCI-H929
Bipolar
Defective
Fraction of spindle state
Vehicle
gNEAT1
ALS
ALS + gNEAT1
C
Top ten enriched processes
Down-regulated biological processes
cellular response to DNA damage stimulus
centromere complex assembly
miotitc cell cycle phase transition
mitotic sister chromatid segregaton
DNA replication
microtubule organization during mitosis
spindle assembly checkpoint signalling
DNA metabolic processes
mitotic spindle organization
DNA repair
Gene count
-log10(p value_normalized)
D
NCAPH
CENPI
SPAG5
KIF14
KIF18A
SPC25
ZWILCH
NUF2
SMC2
KIFC1
SPC24
KNTC1
KIF11
TPX2
NCAPG
TRIP13
CEP192
FBXO5
TTK
SGO1
MAD2L1
CEP55
DLGAP5
CENPK
CENPF
CENPE
CLASP2
BUB1B
SMC4
KIF2C
E
TPX2 gene expression
AMO-1
NCI-H929
gSCR
gNEAT1
TPX2 (100 kDA)
GAPDH (37 kDA)
1
0,47
0,65
TPX2 protein expression
F
AMO-1 SAM
gN#8
ACTIN (42 kDA)
1,5
AMO-1 gSCR
AMO-1 gN#8

Supplementary Methods

Combinatorial strategies targeting NEAT1 and AURKA as new potential therapeutic options for Multiple Myeloma

Authors:

Noemi Puccio[1,2], Gloria Manzotti[1], Elisabetta Mereu[3], FedericaTorricelli[1], Domenica Ronchetti[4], Michela Cumerlato[3], Ilaria Craparotta[5], Laura Di Rito[5], Marco Bolis[5,6], Valentina Traini[4], Veronica Manicardi[1], Valentina Fragliasso[1], Yvan Torrente[7], Nicola Amodio[8], Niccolò Bolli[4,9], Elisa Taiana[9], Alessia Ciarrochi[1], Roberto Piva[3], Antonino Neri[10].

[1]Laboratory of Translational Research, Azienda Unità Sanitaria Locale-IRCCS Reggio Emilia, Reggio Emilia; [2]Clinical and Experimental Medicine PhD Program, University of Modena and Reggio Emilia, Modena; [3]Department of Molecular Biotechnology and Health Sciences, University of Turin, Turin, Italy, [4]Department of Oncology and Hemato-Oncology, University of Milan, Milan, Italy, [5]Computational Oncology Unit, Oncology Department, Mario Negri IRCCS, Milan, [6]Bioinformatics Core Unit, Institute of Oncology Research (IOR), Bellinzona, Switzerland.; Università della Svizzera Italiana, Faculty of Biomedical Sciences, 6900 Lugano, Switzerland, [7]Stem Cell Laboratory, Department of Pathophysiology and Transplantation, University of Milan, Centro Dino Ferrari, Unit of Neurology, Fondazione IRCCS Cà Granda Ospedale Maggiore Policlinico, 20122 Milan, Italy; Novystem Spa, Milan, [8]Department of Experimental and Clinical Medicine, Magna Graecia University of Catanzaro, Catanzaro, [9]Hematology, Fondazione IRCCS Cà Granda Ospedale Maggiore Policlinico, Milan, Italy, [10]Scientific Directorate, Azienda USL-IRCCS Reggio Emilia, 42123 Reggio Emilia, Italy.

Gymnosis

Cells were seeded at low plating density (5×10^4/ml) and concurrently treated with the naked gapmeR NEAT1 (gNEAT1) and the scrambled (gSCR), at a final concentration of 1.5, 2.5, 5, 7 μM. Table showing the LNA-gapmeRs used:

Name	Sequence (5' - 3')	Mw calc (Da)
gNEAT1	AGTGACCACAAAAGGT	5276.2
gSCR	GCTCCCTTCAATCCAA	5184.2

Drug synergism analysis

For HT experiments, Growth Rate (GR) was calculated as the ratio between luminescence values at the two time points, normalized to DMSO-treated cells. Combined drug effect was determined by Excess over Bliss (EOB) analysis on GR value for all concentrations, according to the formula:

EOB=[1−GR(combination)]−[1−GR(DMSO)]−[1−GR(drug)]+[1−GR(DMSO)][1−GR(drug)]^2. EOB cut off >0.2 was used to select the most synergistic drugs (TOP35) in combination with NEAT1 KD.

During the validation step, drug combination studies and synergy quantification were realized with CompuSyn software based on Chou-Talalay method that calculates the combination index (CI). Dose-effect curves were determined by counting viable cells after 72 hours of Alisertib and AURKAi-I treatment and 96 hours after NEAT1 silencing. At least three different concentrations of each drug were combined to two concentrations of gNEAT1 gapmeR (2,5 – 7 μM)

Cell cycle analysis

Cell cycle analyses were performed in AMO-1, NCI-H929 and MM1.S cells after 24 hours of Alisertib and AURKAi-I treatments. Cells were analyzed with the hypotonic propidium iodide (PI) method[1] and samples were acquired with FACS Canto II Cell Analyzer (BD Biosciences).

Cell viability assessment

MM cells proliferation was assessed through Trypan-exlusion method and live cell imaging.

Live cell imaging and analysis

For proliferation assays, cells were seeded in coated 96-well plates (4000 cells/well). Cell coating was performed using 50 µL of 0.005% Poly-L-ornithine solution per well. The plate was incubated for 1 hour at room temperature then, poly-L-ornithine solution was removed from the well to allow the plate to dry for 15 minutes. Cells were stained for 20 minutes at 37 °C using 0,5 µM Citolight Red (4706) (Sartorius AG, Goettingen, Germany), resuspended in PBS 1X. Then, cells were centrifuged at 900 rpm for 5 minutes and resuspended in the appropriate amount of standard medium supplemented with different drugs.

Cell proliferation analysis was performed with the Incucyte® Live-Cell Analysis Systems (Model S3; Sartorius AG, Goettingen, Germany). Cells were imaged within 20 minutes of plating using phase contrast and red (400 ms exposure) image channels in the Incucyte® platform. Five images from distinct regions per well using a 10x dry objective lens were taken every 8 hours. Independent experimental condition was run in triplicates. The IncuCyte software's analysis definition was set to recognize red-stained cells. Top-Hat segmentation method was used for background correction. For accurate quantification of closely spaced objects edge split tool was used. Cell objects count was finalized by applying specific filter for each cell line: $<120\ \mu m^2$ for AMO-1 and for NCI-H929 and $<110\ \mu m^2$ for MM1.S cells. Red object counts per image, for all the five images acquired in each independent technical replicate were used to determine the average number of cells per well.

RNA extraction, reverse transcription and quantitative PCR

Total RNA was extracted using RNeasy kit (Qiagen) according to manufacturer's instructions. The purity and concentration of total RNA was determined by the NanoDrop 1000 spectrophotometer (Thermo Fisher Scientific). The ratios of absorption (260 nm/280 nm) of all samples were between 1.8 and 2.0. 500 ng of total RNA was retrotranscribed with iScript cDNA kit (Bio-Rad, Hercules, California, USA). Quantitative Real-Time PCR (qRT-PCR) was performed for 40 cycles using Sso Fast EvaGreen Super Mix (Bio-Rad, Hercules, California, USA) in a CFX96 Real Time PCR Detection System (Bio-Rad, Hercules, CA, USA). Relative expression of target genes was calculated using the $2^{-\Delta\Delta Ct}$ method by normalizing to the

housekeeping gene expression. To determine transcript levels by qPCR, the following primers were used:

Primer Name	Sequence (5’ – 3’)
Total NEAT1_FW	5' - GCCTTGTAGATGGAGCTTGC - 3'
Total NEAT1_RW	5' - GCACAACACAATGACACCCT - 3'
TPX2_FW	5’ – TTCAAGGCTCGTCCAAACACCG -3’
TPX2_RW	5’ – GCTCTCTTCTCAGTAGCCAGCT -3’
GAPDH_FW	5’ – ACAGTCAGCCGCATCTTCTT – 3’
GAPDH_RW	5’ – AATGAAGGGGTCATTGATGG – 3’
ACTIN_FW	5’ - TGCGTTACACCCTTTCTTGA – 3'
ACTIN_RW	5’ - AAAGCCATGCCAATCTCATC – 3'
FOXM1_FW	5’ – TCTGCCAATGGCAAGGTCTCCT - 3’
FOXM1_RW	5’ – CTGGATTCGGTCGTTTCTGCTG – 3’
KIF11_FW	5’ – ACAGCTGACATGGATGGGAA - 3’
KIF11_R	5’ – TCTGAAAGCTGGATGTGGGT – 3’
NUF2_FW	5’ – CTGCTTCCAAACCATGCACT – 3’
NUF2_RW	5’ – AAAATCCCAGCTGCACAAGG – 3’
CLASP2_FW	5’ – CTGTTAGTGCCATGCGAGTC – 3’
CLASP2_RW	5’ – TTCTGCCACATCTTCCGTCT – 3’
AURKA_FW	5’ – TCCTGAGGAGGAACTGGCATCAAA – 3’
AURKA_RW	5’ – TACCCAGAGGGCGACCAATTTCAA – 3’
INCEP_FW	5’ - AGGCTCCTGAATGTTGAGGTGC – 3’
INCEP_RW	5’ - GTGTGCTGTTGGCAATCTCCGT – 3’

E2F1_FW	5’ – AGCTGGACCACCTGATGAAT – 3’
E2F1_RW	5’ – GAGGGGCTTTGATCACCATA – 3’
PRKCA_FW	5’ – GCCTATGGCGTCCTGTTGTATG – 3’
PRKCA_RW	5’ – GAAACAGCCTCCTTGGACAAGG – 3’
KIF23_FW	5’- GTAGCAAGACCTGTAGACAAGGC – 3’
KIF23_RW	5’ – TTCGCATGACGGCAAAGGTGGA – 3’
EXO-1 FW	5’ – AGCTACGCTGGGCAATATGT - 3’
EXO-1_RW	5’ – ACTTCTTGAATGGGCAGGCA – 3’
FEN1_FW	5’ – AGTGGAGCGAGCCAAATGAA – 3’
FEN1_RW	5’ – TACTCAGCCTCTTGACCCCA – 3’
BRCA1_FW	5’ – GTCCCATCTGTCTGGAGTTGA – 3’
BRCA1_RW	5’ – GGCCCTTTCTTCTGGTTGAGA – 3’
HELLS_FW	5’ – AGCGGTTGTGAGGAGTTAGC – 3’
HELLS_RW	5’ – CATGCCTGGACACTCACCC – 3’
CDC6_FW	5’ – AAGCTGTCTCGGGCATTGAA – 3’
CDC6_RW	5’ – GCTGAGAGGCAGGGCTTTTA – 3’
POLD1_FW	5’ – AAACGCTGTTTGAAGCGGCA – 3’
POLD1_RW	5’ – GAGGTGCATCATCATCATCCCA – 3’

Western blot analysis

Cells were homogenized with PLB lysis buffer (Promega, Madison, WI, USA) supplemented with Protease Inhibitors cocktail (Bimake, Houston, TX, USA). 25-40 µg of total cell lysate were separated using SDS–PAGE using Bio-Rad apparatus (Bio-Rad, Hercules, CA, USA)

with precast Any kD Acriliamide Gels (Bio-Rad, Hercules, CA, USA), electro-transferred onto nitrocellulose membranes (Bio-Rad, Hercules, CA, USA). Membranes were blocked with 5% milk-PBST for at least 2 hours and then immunoblotted with primary antibodies overnight at 4°C in BSA 2%-PBS Tween 0.1% (PBST). Membranes were washed three times in PBST solution and then incubated with a secondary antibody diluted in milk 2% - PBST for 2 hours at room temperature. Chemiluminescence was detected using WESTAR ECL substrate for western blotting (Cyanagen) and the ChemiDoc MP System (Bio-Rad).

The experiments were repeated at least three times.

The table below reported the antibody used:

Antibody	Company	Code	Source	Dilution
Anti-AURKA	Cell signalling technology	14475	Rabbit pAb	1:1000 BSA 2%-PBST
Anti-pAURKA Thr 288	Cell signalling technology	3079	Rabbit pAb	1:500 BSA 2%-PBST
Anti-PLK1	Cell signalling technology	4513	Rabbit pAb	1:1000 BSA 2%-PBST
Anti-CCNB1 (Anti-CycB1)	Santa Cruz Biotechnology	sc-245	Mouse mAb	1:500 BSA 2%-PBST
Anti-TPX2	Cell signalling technology	12245	Rabbit pAb	1:1000 BSA 2%-PBST
Anti-GAPDH	Cell signalling technology	12245	Rabbit pAb	1:2000 BSA 2%-PBST
Anti-ACTIN	Santa Cruz Biotechnology	sc-8432	Mouse mAb	1:2000 BSA 2%-PBST
Anti-mouse IgG	Amersham	NXA931	HRP-linked	1:2000-1:5000 milk 2%-PBST
Anti-rabbit IgG	Amersham	NA934	HRP-linked	1:2000-1: 5000 milk 2%-PBST

Immunofluorescence

0,15 x 10^6 cells for each condition were harvested, immobilized onto glass slides through Cytospin (Thermo Scientific), fixed in 4% paraformaldehyde in PBS for 7 minutes at 22°C, then washed three times with PBS. Cells were permeabilized (0.5% Triton X-100 in PBS) for 15 minutes, washed three times with PBS and blocked for 1 hour at 22°C with 1.5% BSA in PBS. After blocking, slides were washed three times in PBS and incubated for 1 hour at 22°C in the dark with Anti-α-Tubulin Alexa Fluor 488 (Abcam; #185031, 1:100) to stain microtubules. After three PBS washes nuclei staining was performed with DAPI (Sigma-Aldrich) and mounted under coverslips with Glycerol-PBS mounting media. Images were acquired by Leica TCS SP8 confocal laser scanning microscope (DMi8); acquisitions were performed with 63X immersion oil objectives. Conversion of imaged z-stacks into average intensity projections were processed by Leica Microsystem software (Leica Application Suite X - LAS X).

Sequencing and DEG analysis

Before library preparation, RNA concentration was evaluated through Qubit™ RNA Broad Range Assay Kit (Invitrogen, Walthman, MA, USA) while RNA quality was established on 4200 Tapestation (Agilent Technologies, Santa Clara, CA, USA) using RNA Screen tape kit (Agilent Technologies, Santa Clara, CA, USA). According to the TruSeq Stranded Total RNA (San Diego, CA, USA) protocol, 500 ng of RNA for each sample with RIN value between 9 and 10, were used for RNA sequencing. Final libraries with optimal quality and quantity criteria, assessed by D1000 Screen tape kit (Agilent Technologies) and by Qubit® dsDNA High Sensitivity Assay Kit (Invitrogen). Sequencing read quality was assessed with FastQC (v.0.11.9)[3]. Total-RNA (stranded) sequences were aligned to the reference human genome (GRCh38) using STAR (v.2.7.9a)[4] in two-pass mode. Gene expression was quantified at the gene level, utilizing comprehensive annotations from Gencode (v38 GTF File). Samples were normalized and adjusted for library size using the variance stabilizing transformation in the R statistical environment via the DESeq2 (v1.28.1)[5] pipeline. Differential expression analysis between groups employed the embedded Independent Filtering procedure to exclude genes with low expression across most samples. Unless specified otherwise, limma (v.3.44.3) package was used for GSEA (Camera, use ranks set to FALSE), and geneset collections were obtained from the Molecular Signature Database (MSigDB)[6]. P-values underwent false discovery rate (FDR) correction (threshold: 0.05) for multiple testing. Data are available at ArrayExpress; access code: E-MTAB-13925.

Enrichment analysis

Biological processes analyses were performed by EnrichR enrichment website tool (https://maayanlab.cloud/Enrichr/).Genes from differential expression analyses with a fold change ≤ - 0,7 and padj ≤ 0,05 were used to identify GO and pathways (n = 88) and were used to perform GO and pathways analyses Enriched biological processes were considered significant by applying a threshold of 0.05 on *p*-value adjusted by Benjamini-Hochberg correction for multiple testing.

Connectivity Map

Differential gene expression signature obtained comparing AMO-1_NEAT1 KD and AMO-1_SCR cells, was used as input of the Connectivity Map (cMap, v1.1.1.43, dataset v1.1.1.2, accessed via https://clue.io). cMAP output is list of perturbagenes (pharmacological and genetic strategies - the latter not considered in this study) ranked according to the similarity between the input and the signature they induce in a set of cell lines.

Since at the time of our query, none of the cell lines present on the cMap database were of multiple myeloma cells, we used the option "summary" which, given a set of connectivity scores for a particular inhibitor, summarizes those scores across all the eight cell lines tested. Compounds presenting a similar transcriptional signature to our query were selected considering a connectivity score > 90.

Multi-Omics Data in CoMMpass Study

Multi-omics data about bone marrow MM samples at baseline (BM_1) were publicly accessible from MMRF CoMMpass Study (https://research.themmrf.org/) including more than 1000 MM patients from several worldwide sites and retrieved from the Interim Analysis 20 (MMRF_CoMMpass_IA20, accessed on 19 January 2023). Transcript per Million (TPM) reads values of the AURKA transcript were retrieved using Salmon gene expression quantification data (MMRF_CoMMpass_IA20_salmon_geneUnstranded_TPM) in 767 BM_1 MM patients. Clinical data regarding Overall Survival (OS) and Progression free Survival (PFS) were considered in 767 MM patients for which both RNA-seq expression and survival data were available. Non-synonymous (NS) somatic mutation variants and counts data were obtained from whole exome sequencing (WES) analyses, main IgH translocations were inferred from

RNA-seq spike expression estimates of known target genes and Copy Number Alteration (CNA) data were retrieved by means of Next generation Sequencing (NGS)-based fluorescence in situ hybridization (FISH)[7] in 489 MM cases for which all data were available[8]. The presence of a specific CNA was considered when occurring in at least one of the investigated cytoband at a 20% cut-off for each considered chromosomal aberration, as previously reported[7].

Survival analyses

Survival analyses were performed using survival[9,10] and survminer[11] packages in R Bioconductor (version 4.1.2). Kaplan-Meier analysis was applied on OS and PFS data in patients stratified in quartiles and by comparing the first and fourth quartiles. Log-Rank test p-value was calculated to measure the global difference between survival curves. Cox proportional hazards model was applied as univariate analysis on single molecular variables, age and International Staging System (ISS) groups in relation to OS and PFS data in 489 MM cases for which all information were accessible. Cox regression multivariate analysis was applied on all significant features after BH correction. Forest plot was used to summarize Cox Proportional Hazard Model.

Statistical analysis

For functional assays statistical analysis was performed using GraphPad Prism Software (version 9.5.1 for Windows, GraphPad Software, San Diego, CA, USA). Statistical significance was determined using the Student's *t*-test. Differences were considered significant when *P* values were **P*<0.05, ***P*<0.01 or ****P*<0.001.

Supplementary methods references

1.Riccardi, C. and Nicoletti, I. (2006) Analysis of Apoptosis by Propidium Iodide Staining and Flow Cytometry. http://www.natureprotocols.com.

2. Mereu E, Abbo D, Paradzik T, Cumerlato M, Bandini C, Labrador M, Maccagno M, Ronchetti D, Manicardi V, Neri A, et al. Euchromatic Histone Lysine Methyltransferase 2 Inhibition Enhances Carfilzomib Sensitivity and Overcomes Drug Resistance in Multiple Myeloma Cell Lines. *Cancers*. 2023; 15(8):2199.

3.Andrews, S. Babraham Bioinformatics - FastQC A Quality Control tool for High Throughput Sequence Data. https://www.bioinformatics.babraham.ac.uk/projects/fastqc/ (2010).

4.Dobin, A. *et al.* STAR: ultrafast universal RNA-seq aligner. *Bioinformatics* **29**, 15–21 (2013).

5.Love, M. I., Huber, W. & Anders, S. Moderated estimation of fold change and dispersion for RNA-seq data with DESeq2. *Genome Biology* **15**, 550 (2014).

6.Liberzon, A. *et al.* The Molecular Signatures Database (MSigDB) hallmark gene set collection. *Cell Syst* **1**, 417–425 (2015).

7.Miller, C. et al. A comparison of clinical FISH and sequencing based FISH estimates in multiple myeloma: An MMRF CoMMpass analysis. In: Hematology TASo, editor. The American Society of Hematology; 2016: Blood; 2016. p. 374.

8.Todoerti K, Ronchetti D, Favasuli V, Maura F, Morabito F, Bolli N, Taiana E, Neri A. DIS3 mutations in multiple myeloma impact the transcriptional signature and clinical outcome. Haematologica. 2021.

9.Therneau T (2021). A Package for Survival Analysis in R_. R package version 3.2-11, <URL: https://CRAN.R-project.org/package=survival>.

10.Terry M. Therneau, Patricia M. Grambsch (2000). _Modeling Survival Data: Extending the Cox Model_. Springer, New York. ISBN 0-387-98784-3.

11.Alboukadel Kassambara, Marcin Kosinski and Przemyslaw Biecek (2021). survminer: Drawing Survival Curves using 'ggplot2'. R package version 0.4.9. https://CRAN.R-project.org/package=survminer.

Supplementary table 1

Cat n°	Drug	Target	Pathway
S2698	RS-127445	5-HT Receptor	Neuronal Signaling
S2894	SB742457	5-HT Receptor	Neuronal Signaling
S1549	Nebivolol HCl	Adrenergic Receptor	Neuronal Signaling
S8114	ICI-118551 Hydrochloride	Adrenergic Receptor	GPCR & G Protein
S1078	MK-2206 2HCl	Akt	PI3K/Akt/mTOR
S2808	Ipatasertib (GDC-0068)	Akt	PI3K/Akt/mTOR
S4854	Bedaquiline fumarate	Anti-infection	Microbiology
S1188	Anastrozole	Aromatase	Endocrinology & Hormones
S8292	Selonsertib (GS-4997)	ASK	Apoptosis
S1092	KU-55933 (ATM Kinase Inhibitor)	ATM/ATR	DNA Damage
S1570	KU-60019	ATM/ATR	DNA Damage
S7102	VE-822	ATM/ATR	PI3K/Akt/mTOR
S8556	AZ31	ATM/ATR	DNA Damage
S8666	BAY 1895344 (BAY-1895344)	ATM/ATR	DNA Damage
S8680	AZD1390	ATM/ATR	PI3K/Akt/mTOR
S1048	Tozasertib (VX-680, MK-0457)	Aurora Kinase	Cell Cycle
S1133	Alisertib (MLN8237)	Aurora Kinase	Cell Cycle
S1147	Barasertib (AZD1152-HQPA)	Aurora Kinase	Cell Cycle
S1451	Aurora A Inhibitor I	Aurora Kinase	Cell Cycle
S2740	GSK1070916	Aurora Kinase	Cell Cycle
S2770	MK-5108 (VX-689)	Aurora Kinase	Cell Cycle
S7065	MK-8745	Aurora Kinase	Cell Cycle
S2744	CCT137690	Aurora Kinase	Cell Cycle
S1023	Erlotinib HCl (OSI-744)	Autophagy,EGFR	Protein Tyrosine Kinase
S1049	Y-27632 2HCl	Autophagy,ROCK	Cell Cycle
S7849	BDA-366	Bcl-2	Apoptosis
S8048	Venetoclax (ABT-199, GDC-0199)	Bcl-2	Apoptosis
S7790	A-1210477	Bcl-2	Apoptosis
S8591	FX1	Bcl-6	Apoptosis
S2899	GNF-2	Bcr-Abl	Angiogenesis
S2680	Ibrutinib (PCI-32765)	BTK	Angiogenesis
S7173	Spebrutinib (CC-292, AVL-292)	BTK	Angiogenesis
S7257	CNX-774	BTK	Angiogenesis
S7734	LFM-A13	BTK	Angiogenesis
S8777	Evobrutinib	BTK	Protein Tyrosine Kinase
S1094	PF-04217903	c-Met	Protein Tyrosine Kinase

S1114	JNJ-38877605	c-Met	Protein Tyrosine Kinase
S2747	AMG-458	c-Met	Protein Tyrosine Kinase
S2753	Tivantinib (ARQ 197)	c-Met	Protein Tyrosine Kinase
S2761	NVP-BVU972	c-Met	Protein Tyrosine Kinase
S7067	Tepotinib (EMD 1214063)	c-Met	Protein Tyrosine Kinase
S7674	Savolitinib(AZD6094, HMPL-504)	c-Met	Protein Tyrosine Kinase
S8167	AMG 337	c-Met	Protein Tyrosine Kinase
S7564	SAR125844	c-Met	Protein Tyrosine Kinase
S1112	SGX-523	c-Met	Protein Tyrosine Kinase
S2788	Capmatinib (INCB28060)	c-Met	Protein Tyrosine Kinase
S7436	NH125	CaMK	Neuronal Signaling
S7499	ESI-09	cAMP	GPCR & G Protein
S7500	HJC0350	cAMP	GPCR & G Protein
S8012	Otenabant (CP-945598) HCl	Cannabinoid Receptor	GPCR & G Protein
S7461	LDC000067	CDK	Cell Cycle
S7992	LDC4297 (LDC044297)	CDK	Cell Cycle
S8652	Skp2 inhibitor C1 (SKPin C1)	CDK	Cell Cycle
S8727	Atuveciclib (BAY-1143572)	CDK	Cell Cycle
S1116	Palbociclib (PD-0332991) HCl	CDK	Cell Cycle
S1579	Palbociclib (PD0332991) Isethionate	CDK	Cell Cycle
S2626	Rabusertib (LY2603618)	Chk	Cell Cycle
S2683	CHIR-124	Chk	Cell Cycle
S8253	CCT245737	Chk	Cell Cycle
S8632	Chk2 Inhibitor II (BML-277)	Chk	Cell Cycle
S2903	Lumiracoxib	COX	Neuronal Signaling
S4136	Carprofen	COX	Neuronal Signaling
S7725	BLZ945	CSF-1R	Protein Tyrosine Kinase
S8042	GW2580	CSF-1R	Protein Tyrosine Kinase
S7651	SB225002	CXCR	GPCR & G Protein
S8813	LIT-927	CXCR	Immunology & Inflammation
S1115	Odanacatib (MK-0822)	Cysteine Protease	Proteases
S7241	AGI-6780	Dehydrogenase	Metabolism
S8619	NCT-503	Dehydrogenase	Metabolism
S2868	Alogliptin（SYK-322）benzoate	DPP-4	Proteases
S3031	Linagliptin	DPP-4	Proteases

S4002	Sitagliptin phosphate monohydrate	DPP-4	Proteases
S4697	Saxagliptin hydrate	DPP-4	Proteases
S5063	Trelagliptin succinate	DPP-4	Proteases
S5079	Sitagliptin	DPP-4	Proteases
S5365	Alogliptin	DPP-4	Proteases
S5909	Anagliptin	DPP-4	Proteases
S7513	Trelagliptin	DPP-4	Proteases
S8565	Omarigliptin (MK-3102)	DPP-4	Proteases
S7140	TCID	DUB	Ubiquitin
S8047	Dynasore	Dynamin	Cytoskeletal Signaling
S7129	PYR-41	E1 Activating	Ubiquitin
S1173	WZ4002	EGFR	Protein Tyrosine Kinase
S2185	AST-1306	EGFR	Protein Tyrosine Kinase
S7206	CNX-2006	EGFR	Protein Tyrosine Kinase
S7786	Erlotinib	EGFR	Protein Tyrosine Kinase
S8724	Lazertinib (YH25448,GNS-1480)	EGFR	Protein Tyrosine Kinase
S1167	CP-724714	EGFR,HER2	Protein Tyrosine Kinase
S2192	Sapitinib (AZD8931)	EGFR,HER2	Protein Tyrosine Kinase
S1456	Zibotentan (ZD4054)	Endothelin Receptor	GPCR & G Protein
S2097	Ambrisentan	Endothelin Receptor	GPCR & G Protein
S5916	GSK 5959	Epigenetic Reader Do	Epigenetics
S8296	dBET1	Epigenetic Reader Do	Epigenetics
S1216	PFI-1 (PF-6405761)	Epigenetic Reader Domain	Epigenetics
S7110	(+)-JQ1	Epigenetic Reader Domain	Epigenetics
S7620	GSK1324726A (I-BET726)	Epigenetic Reader Domain	Epigenetics
S7835	I-BRD9	Epigenetic Reader Domain	Epigenetics
S7906	PFI-4	Epigenetic Reader Domain	Epigenetics
S8180	PF-CBP1 HCl	Epigenetic Reader Domain	Epigenetics
S8190	CPI-637	Epigenetic Reader Domain	Epigenetics
S8265	GSK6853	Epigenetic Reader Domain	Epigenetics
S7525	XMD8-92	ERK	MAPK
S7709	VX-11e	ERK	MAPK
S8534	LY3214996	ERK	MAPK
S2631	URB597	FAAH	Metabolism
S2666	PF-3845	FAAH	Metabolism
S2828	JNJ-1661010	FAAH	Metabolism
S1593	Apixaban	Factor Xa	Metabolism
S3002	Rivaroxaban	Factor Xa	Metabolism

S7167	SSR128129E	FGFR	Angiogenesis
S8493	PD-166866 (PD166866)	FGFR	Angiogenesis
S8503	BLU-554 (BLU554)	FGFR	Angiogenesis
S8675	H3B-6527	FGFR	Protein Tyrosine Kinase
S8548	FGF401	FGFR	Protein Tyrosine Kinase
S8023	TCS 359	FLT3	Angiogenesis
S2861	CTEP (RO4956371)	GluR	Neuronal Signaling
S2251	(-)-Huperzine A (HupA)	GluR,AChR	Neuronal Signaling
S8452	BAY-876	GLUT	Metabolism
S7753	BPTES	Glutaminase	Proteases
S7263	AZD1981	GPR	Endocrinology & Hormones
S1263	CHIR-99021 (CT99021)	GSK-3	PI3K/Akt/mTOR
S2729	SB415286	GSK-3	PI3K/Akt/mTOR
S2745	CHIR-98014	GSK-3	PI3K/Akt/mTOR
S2924	CHIR-99021 (CT99021) HCl	GSK-3	PI3K/Akt/mTOR
S7063	LY2090314	GSK-3	PI3K/Akt/mTOR
S7193	1-Azakenpaullone	GSK-3	PI3K/Akt/mTOR
S7435	AR-A014418	GSK-3	PI3K/Akt/mTOR
S7915	BIO-acetoxime	GSK-3	PI3K/Akt/mTOR
S4935	Asunaprevir	HCV Protease	Proteases
S5402	Dasabuvir(ABT-333)	HCV Protease	Proteases
S2012	PCI-34051	HDAC	Epigenetics
S7229	RGFP966	HDAC	Epigenetics
S7473	Nexturastat A	HDAC	DNA Damage
S7595	Santacruzamate A (CAY10683)	HDAC	DNA Damage
S7596	CAY10603	HDAC	DNA Damage
S2216	Mubritinib (TAK 165)	HER2	Protein Tyrosine Kinase
S2816	Tyrphostin AG 879	HER2	Protein Tyrosine Kinase
S8362	Irbinitinib (ARRY-380, ONT-380)	HER2	Protein Tyrosine Kinase
S2919	IOX2	HIF	Angiogenesis
S2905	JNJ-7777120	Histamine Receptor	Neuronal Signaling
S5926	Pitolisant hydrochloride	Histamine Receptor	Neuronal Signaling
S8776	WM-1119	Histone Acetyltransf	Epigenetics
S4800	Daminozide	Histone Demethylase	Epigenetics
S7574	GSK-LSD1 2HCl	Histone Demethylase	Epigenetics
S7680	SP2509	Histone Demethylase	Epigenetics
S7795	ORY-1001 (RG-6016) 2HCl	Histone Demethylase	Epigenetics
S7079	SGC 0946	Histone Methyltransferase	Epigenetics
S7165	UNC1999	Histone Methyltransferase	Epigenetics
S7230	UNC0642	Histone Methyltransferase	Epigenetics

S7294	PFI-2 HCl	Histone Methyltransferase	Epigenetics
S7572	A-366	Histone Methyltransferase	Epigenetics
S7575	LLY-507	Histone Methyltransferase	Epigenetics
S7656	CPI-360	Histone Methyltransferase	Epigenetics
S7748	EPZ015666(GSK3235025)	Histone Methyltransferase	Epigenetics
S7820	EPZ020411 2HCl	Histone Methyltransferase	Epigenetics
S7983	A-196	Histone Methyltransferase	Epigenetics
S8340	SGC2085	Histone Methyltransferase	Epigenetics
S8479	LLY-283	Histone Methyltransferase	Epigenetics
S7004	EPZ005687	Histone Methyltransferase	Epigenetics
S7061	GSK126	Histone Methyltransferase	Epigenetics
S7128	Tazemetostat (EPZ-6438)	Histone Methyltransferase	Epigenetics
S7282	NMS-E973	HSP (e.g. HSP90)	Cytoskeletal Signaling
S7751	VER155008	HSP (e.g. HSP90)	Cytoskeletal Signaling
S2695	Nepicastat (SYN-117) HCl	Hydroxylase	Metabolism
S4926	(R)-Nepicastat HCl	Hydroxylase	Metabolism
S8657	PF-06840003	IDO	Metabolism
S1093	GSK1904529A	IGF-1R	Protein Tyrosine Kinase
S7668	Picropodophyllin (PPP)	IGF-1R	Protein Tyrosine Kinase
S8660	GI254023X	Immunology & Inflammation related	Immunology & Inflammation
S7809	MCC950(CP-456773)	Immunology & Inflammation related	Immunology & Inflammation
S2005	Raltegravir (MK-0518)	Integrase	Microbiology
S5245	Raltegravir potassium	Integrase,HIV Protease	Microbiology
S4907	SC-514	IκB/IKK	NF-κB
S8044	BMS-345541	IκB/IKK	NF-κB
S5903	JANEX-1	JAK	JAK/STAT
S8538	PF-06651600	JAK	JAK/STAT
S8541	FM-381	JAK	JAK/STAT
S7508	JNK Inhibitor IX	JNK	MAPK
S8201	BI-78D3	JNK	MAPK
S1452	Ispinesib (SB-715992)	Kinesin	Cytoskeletal Signaling
S2182	SB743921 HCl	Kinesin	Cytoskeletal Signaling
S5933	K 858	Kinesin	Cytoskeletal Signaling
S4904	JZL184	Lipase	Metabolism
S7364	Atglistatin	Lipase	Metabolism
S7457	XEN445	Lipase	Metabolism
S1472	Safinamide Mesylate	MAO	Metabolism
S7875	NVP-CGM097	Mdm2	Apoptosis
S1008	Selumetinib (AZD6244)	MEK	MAPK
S1020	PD184352 (CI-1040)	MEK	MAPK
S1036	PD0325901	MEK	MAPK

S1066	SL-327	MEK	MAPK
S1089	Refametinib (RDEA119, Bay 86-9766)	MEK	MAPK
S1102	U0126-EtOH	MEK	MAPK
S1475	Pimasertib (AS-703026)	MEK	MAPK
S2673	Trametinib (GSK1120212)	MEK	MAPK
S8041	Cobimetinib (GDC-0973, RG7420)	MEK	MAPK
S7430	SB-3CT	MMP	Proteases
S7421	CGP 57380	MNK	MAPK
S7632	TH588	MTH1	DNA Damage
S1226	KU-0063794	mTOR	PI3K/Akt/mTOR
S1266	WYE-354	mTOR	PI3K/Akt/mTOR
S1555	AZD8055	mTOR	PI3K/Akt/mTOR
S2624	OSI-027	mTOR	PI3K/Akt/mTOR
S2689	WAY-600	mTOR	PI3K/Akt/mTOR
S2783	Vistusertib (AZD2014)	mTOR	PI3K/Akt/mTOR
S2811	Sapanisertib (INK 128, MLN0128)	mTOR	PI3K/Akt/mTOR
S7035	XL388	mTOR	PI3K/Akt/mTOR
S7886	CC-223	mTOR	PI3K/Akt/mTOR
S8040	GDC-0349	mTOR	PI3K/Akt/mTOR
S8642	GSK'963	NF-κB,TNF-alpha	NF-κB
S5476	Rolapitant	NK1-receptor	GPCR
S5696	JNJ0966	Others	Others
S7213	Thiamet G	Others	Others
S7270	SRPIN340	Others	Others
S7272	4μ8C	Others	Others
S9360	4-Hydroxyquinazoline	Others	antiplatelet
S1195	TAK-700 (Orteronel)	P450 (e.g. CYP17)	Metabolism
S2921	PF-4981517	P450 (e.g. CYP17)	Metabolism
S3673	Sulfaphenazole	P450 (e.g. CYP17)	Metabolism
S7093	IPA-3	PAK	Cytoskeletal Signaling
S1004	Veliparib (ABT-888)	PARP	DNA Damage
S1060	Olaparib (AZD2281, Ku-0059436)	PARP	DNA Damage
S2741	Niraparib (MK-4827)	PARP	DNA Damage
S7238	NVP-TNKS656	PARP	DNA Damage
S8363	NMS-P118	PARP	DNA Damage
S8592	Pamiparib (BGB-290)	PARP	DNA Damage
S1512	Tadalafil	PDE	Metabolism
S1550	Pimobendan	PDE	Metabolism
S2312	Icariin	PDE	Metabolism
S2687	Mardepodect (PF-2545920)	PDE	Metabolism
S4019	Avanafil	PDE	Metabolism

S5837	BRL-50481	PDE	Metabolism
S2620	GSK256066	PDE	Metabolism
S1536	CP-673451	PDGFR	Protein Tyrosine Kinase
S7087	GSK2334470	PDK	PI3K/Akt/mTOR
S7033	GSK2656157	PERK	Apoptosis
S7307	GSK2606414	PERK	Apoptosis
S7400	ISRIB (trans-isomer)	PERK	Apoptosis
S8278	SHP099 dihydrochloride	phosphatase	Others
S2717	CP-91149	Phosphorylase	Metabolism
S1169	TGX-221	PI3K	PI3K/Akt/mTOR
S1352	TG100-115	PI3K	PI3K/Akt/mTOR
S2636	A66	PI3K	PI3K/Akt/mTOR
S5818	acalisib (GS-9820)	PI3K	PI3K/Akt/mTOR
S7335	IPI-3063	PI3K	PI3K/Akt/mTOR
S7938	GSK2292767	PI3K	PI3K/Akt/mTOR
S7980	VPS34-IN1	PI3K	PI3K/Akt/mTOR
S8330	IPI-549	PI3K	PI3K/Akt/mTOR
S8456	VPS34 inhibitor 1 (Compound 19, PIK-III analogue)	PI3K	PI3K/Akt/mTOR
S8581	Serabelisib (INK-1117,MLN-1117,TAK-117)	PI3K	PI3K/Akt/mTOR
S8672	Tenalisib (RP6530)	PI3K	PI3K/Akt/mTOR
S8005	SMI-4a	Pim	JAK/STAT
S7208	Bisindolylmaleimide I (GF109203X)	PKC	TGF-beta/Smad
S1109	BI 2536	PLK	Cell Cycle
S2193	GSK461364	PLK	Cell Cycle
S7248	Ro3280	PLK	Cell Cycle
S7255	NMS-P937 (NMS1286937)	PLK	Cell Cycle
S7720	SBE 13 HCl	PLK	Cell Cycle
S2871	T0070907	PPAR	DNA Damage
S7767	AZ6102	PPAR	DNA Damage
S2224	UK 383367	Procollagen C Proteinase	Metabolism
S7462	PI-1840	Proteasome	Proteases
S8651	bpV (HOpic)	PTEN	Others
S3057	Azilsartan Medoxomil	RAAS	Endocrinology & Hormones
S4102	Eprosartan Mesylate	RAAS	Endocrinology & Hormones
S5069	Dabrafenib Mesylate	Raf	MAPK
S7964	PLX7904	Raf	MAPK
S8745	LXH254	Raf	MAPK
S8031	NSC 23766	Rho	Cell Cycle
S1474	GSK429286A	ROCK	Cell Cycle
S8489	GSK180736A (GSK180736)	ROCK	Cell Cycle

S7176	SKI II	S1P Receptor	GPCR & G Protein
S7177	PF-543	S1P Receptor	GPCR & G Protein
S7218	Alvelestat (AZD9668)	Serine Protease	Proteases
S8457	UK-371804 HCl	Serine Protease	Proteases
S8465	GSK'872 (GSK2399872A)	Serine/threonin kinase	Apoptosis
S7188	CID755673	Serine/threonin kinase,CaMK	Apoptosis
S1548	Dapagliflozin	SGLT	GPCR & G Protein
S2760	Canagliflozin	SGLT	GPCR & G Protein
S5566	Dapagliflozin propanediol monohydrate	SGLT	GPCR & G Protein
S5901	Canagliflozin hemihydrate	SGLT	GPCR & G Protein
S8022	Empagliflozin (BI 10773)	SGLT	GPCR & G Protein
S8558	Tofogliflozin(CSG 452)	SGLT	GPCR & G Protein
S8637	Ipragliflozin (ASP1941)	SGLT	GPCR & G Protein
S5413	Ertugliflozin	SGLT2	Ion-Channel
S1541	Selisistat (EX 527)	Sirtuin	Epigenetics
S2804	Sirtinol	Sirtuin	Epigenetics
S7845	SirReal2	Sirtuin	Epigenetics
S8245	Thiomyristoyl	Sirtuin	DNA Damage
S2785	A-803467	Sodium Channel	Transmembrane Transporters
S2285	Cryptotanshinone	STAT	JAK/STAT
S7024	Stattic	STAT	JAK/STAT
S7501	HO-3867	STAT	JAK/STAT
S1189	Aprepitant	Substance P	Others
S7006	BAY-61-3606	Syk	Angiogenesis
S1186	BIBR 1532	Telomerase	DNA Damage
S1067	SB431542	TGF-beta/Smad	TGF-beta/Smad
S7146	DMH1	TGF-beta/Smad	TGF-beta/Smad
S7624	SD-208	TGF-beta/Smad	TGF-beta/Smad
S7959	SIS3 HCl	TGF-beta/Smad	TGF-beta/Smad
S7507	LDN-193189 2HCl	TGF-beta/Smad	TGF-beta/Smad
S7148	ML347	TGF-beta/Smad,ALK	TGF-beta/Smad
S5074	Argatroban Monohydrate	Thrombin	Others
S1577	Tie2 kinase inhibitor	Tie-2	Protein Tyrosine Kinase
S8677	Cu-CPT22	TLR	Immunology & Inflammation
S8641	Nec-1s (7-Cl-O-Nec1)	TNF-alpha	Apoptosis
S8787	GSK'547	TNF-alpha	Apoptosis
S7465	FTI 277 HCl	Transferase	Metabolism
S2891	GW441756	Trk receptor	Protein Tyrosine Kinase
S7960	Larotrectinib (LOXO-101) sulfate	Trk receptor	Protein Tyrosine Kinase

S2773	SB705498	TRPV	Others
S8238	SB366791	TRPV	Transmembrane Transporters
S5623	Bedaquiline	tuberculosis	Immunology
S2896	ZM 323881 HCl	VEGFR	Protein Tyrosine Kinase
S5667	Fruquintinib	VEGFRs	VEGFR
S9500	Valbenazine tosylate	VMAT2	Others
S1525	Adavosertib （MK-1775）	Wee1	Cell Cycle
S2662	ICG-001	Wnt/beta-catenin	Stem Cells & Wnt
S8327	KYA1797K	Wnt/beta-catenin	Stem Cells & Wnt
S8644	GNF-6231	Wnt/beta-catenin	Stem Cells & Wnt

Supplementary table 1. List of drugs used for the high-throughput screening.

Supplementary table 2

		IC 50 (72 hous)
Alisertib	AMO-1	32 nM
	NCI-H929	18 nM
	MM1.S	10 nM

		IC 50 (72 hous)
AURKAi-I	AMO-1	0,28 µM
	NCI-H929	0,2 µM
	MM1.S	0,11 µM

Supplementary table 2. IC50 calculation at 72 hours of Alisertib and AURKAi for AMO-1, NCI-H929 and MM1.S cell lines.

Supplementary table 3

Gene ID	Gene name	Gene type	Fold change	p adj value
ENSG00000174442	ZWILCH	protein coding	-2,33	4,14E-132
ENSG00000138160	KIF11	protein coding	-1,54	2,07E-66
ENSG00000163539	CLASP2	protein coding	-1,21	8,12E-106
ENSG00000143228	NUF2	protein coding	-1,11	2,38E-32
ENSG00000161888	SPC24	protein coding	-1,01	2,18E-42
ENSG00000088325	TPX2	protein coding	-0,96	1,05E-74
ENSG00000123219	CENPK	protein coding	-0,94	6,13E-14
ENSG00000117724	CENPF	protein coding	-0,93	6,36E-39
ENSG00000152253	SPC25	protein coding	-0,92	8,91E-14
ENSG00000126787	DLGAP5	protein coding	-0,92	9,11E-26
ENSG00000102384	CENPI	protein coding	-0,92	1,61E-22
ENSG00000112029	FBXO5	protein coding	-0,88	8,72E-26
ENSG00000156970	BUB1B	protein coding	-0,87	2,03E-42
ENSG00000142945	KIF2C	protein coding	-0,86	1,03E-49
ENSG00000112742	TTK	protein coding	-0,85	3,44E-18
ENSG00000118193	KIF14	protein coding	-0,83	1,15E-22
ENSG00000129810	SGO1	protein coding	-0,81	2,27E-18
ENSG00000121152	NCAPH	protein coding	-0,81	1,50E-33
ENSG00000101639	CEP192	protein coding	-0,81	3,96E-39
ENSG00000138778	CENPE	protein coding	-0,80	4,36E-07
ENSG00000237649	KIFC1	protein coding	-0,80	3,27E-33
ENSG00000076382	SPAG5	protein coding	-0,79	3,17E-38
ENSG00000164109	MAD2L1	protein coding	-0,79	2,56E-14
ENSG00000109805	NCAPG	protein coding	-0,79	3,01E-21
ENSG00000138180	CEP55	protein coding	-0,77	1,17E-24
ENSG00000071539	TRIP13	protein coding	-0,76	4,53E-41
ENSG00000136824	SMC2	protein coding	-0,76	1,28E-19
ENSG00000121621	KIF18A	protein coding	-0,75	3,56E-15
ENSG00000184445	KNTC1	protein coding	-0,74	2,24E-24
ENSG00000113810	SMC4	protein coding	-0,71	6,56E-17

Supplementary table 3. List of top-thirty significant down-regulated genes belonging to mitotic spindle and microtubule organization (GO:0007052; GO:1902850) in AMO-1 NEAT1 KD cells compared to the scramble condition. Down-regulated genes are ordered according to the fold change.

Supplementary table 4

IgH trx (RNA-seq)	N (%)
t(11;14)/CCND1	136 (20.6%)
t(6;14)/CCND3	9 (1.4%)
t(4;14)/WHSC1/FGFR3	89 (13.5%)
t(14;16)/MAF;t(14;20)/MAFB; t(8;16)/MAFA	42 (6.4%)
t(8;14)/MYC	27 (4.1%)
CNA (FISH-WES)	**N (%)**
del(13)(q14)/(q34)/RB1_20%	346 (52.4%)
1q21 gain_20%	240 (36.4%)
del(1)(p22)/CDKN2C_20%	199 (30.2%)
del(17)(p13)/TP53_20%	74 (11.2%)
HD	375 (56.8%)
NS Somatic Mutation (WES)	**N (%)**
DIS3	71 (10.8%)
N-RAS	146 (22.1%)
H-RAS	0 (0%)
K-RAS	160 (24.2%)
BRAF	51 (7.7%)
TP53	30 (4.5%)
FAM46C	66 (10%)
TRAF3	50 (7.6%)

Supplementary Table 4. Number and relative frequency of main IgH translocations (trx), copy number alterations (CNAs) and non-synonymous (NS) somatic mutations, in 660 BM-1 MM cases of MMRF_CoMMpass_IA20 cohort with available data about AURKA expression by RNA sequencing (RNA -seq), IgH trx by RNA-seq, NS somatic mutations by Whole Exome sequencing (WES) and CNAs by next generation sequencing (NGS)-based FISH (FISH-WES).

Supplementary table 5

A

Variable	N (%)	OS Univariate Cox Analysis		
		HR (95% CI)	P-value	Adj. P-value
high *AURKA*	247 (50)	1.54 (1.11-2.13)	0.0102	0.0306*
Age (≥ 65 yrs)	206 (41)	2.12 (1.46-3.08)	0.0000868	0.0005***
ISS I	187 (38)	0.31 (0.19-0.50)	0.00000186	0.0000195****
ISS II	171 (34)	1.13 (0.78-1.64)	0.524	0.687
ISS III	139 (28)	2.45 (1.70-3.53)	0.00000162	0.0000195****
del(1p)/CDKN2C	143 (29)	1.61 (1.10-2.35)	0.0148	0.0347*
del(13q)/RB1	258 (52)	2.11 (1.44-3.09)	0.000119	0.0005***
HD	281 (56)	0.64 (0.44-0.92)	0.0149	0.0347*
TP53.alterations	40 (8)	1.05 (0.53-2.07)	0.892	0.892
1q21 gain/amp	164 (33)	1.68 (1.17-2.43)	0.0051	0.0178*
TP53.alterations + 1q21 gain/amp	19 (4)	3.63 (1.89-6.97)	0.000103	0.0005***
DIS3 mut	50 (10)	1.63 (1.06-2.50)	0.0264	0.052
N-RAS mut	117 (23)	0.90 (0.62-1.32)	0.596	0.732
K-RAS mut	121 (24)	1.07 (0.77-1.49)	0.694	0.762
BRAF mut	36 (7)	1.18 (0.60-2.31)	0.628	0.732
FAM46C mut	49 (10)	0.78 (0.42-1.43)	0.419	0.586
TRAF3 mut	38 (7)	0.42 (0.17-1.06)	0.0668	0.107
t(11;14)	102 (20)	0.92 (0.58-1.46)	0.726	0.762
t(4;14)	69 (14)	1.63 (1.04-2.55)	0.0335	0.058
MAF.trx	33 (7)	1.96 (1.08-3.57)	0.0276	0.052
MYC.trx	20 (4)	1.92 (0.94-3.94)	0.0748	0.112

B

Variable	N (%)	OS Univariate Cox Analysis		
		HR (95% CI)	P-value	Adj. P-value
high *AURKA*	247 (50)	1.54 (1.11-2.13)	0.0102	0.0306*
Age (≥ 65 yrs)	206 (41)	2.12 (1.46-3.08)	0.0000868	0.0005***
ISS I	187 (38)	0.31 (0.19-0.50)	0.00000186	0.0000195****
ISS II	171 (34)	1.13 (0.78-1.64)	0.524	0.687
ISS III	139 (28)	2.45 (1.70-3.53)	0.00000162	0.0000195****
del(1p)/CDKN2C	143 (29)	1.61 (1.10-2.35)	0.0148	0.0347*
del(13q)/RB1	258 (52)	2.11 (1.44-3.09)	0.000119	0.0005***
HD	281 (56)	0.64 (0.44-0.92)	0.0149	0.0347*
TP53.alterations	40 (8)	1.05 (0.53-2.07)	0.892	0.892
1q21 gain/amp	164 (33)	1.68 (1.17-2.43)	0.0051	0.0178*
TP53.alterations + 1q21 gain/amp	19 (4)	3.63 (1.89-6.97)	0.000103	0.0005***
DIS3 mut	50 (10)	1.63 (1.06-2.50)	0.0264	0.052
N-RAS mut	117 (23)	0.90 (0.62-1.32)	0.596	0.732
K-RAS mut	121 (24)	1.07 (0.77-1.49)	0.694	0.762
BRAF mut	36 (7)	1.18 (0.60-2.31)	0.628	0.732
FAM46C mut	49 (10)	0.78 (0.42-1.43)	0.419	0.586
TRAF3 mut	38 (7)	0.42 (0.17-1.06)	0.0668	0.107
t(11;14)	102 (20)	0.92 (0.58-1.46)	0.726	0.762
t(4;14)	69 (14)	1.63 (1.04-2.55)	0.0335	0.058
MAF.trx	33 (7)	1.96 (1.08-3.57)	0.0276	0.052
MYC.trx	20 (4)	1.92 (0.94-3.94)	0.0748	0.112

Supplementary table 5. Results of Cox regression univariate analysis using OS (**A**) or PFS (**B**) data on AURKA expression groups, age equal to or greater than 65 years, ISS subgroups and main molecular alterations in 489 BM-1 MM cases for which all data were available. Number (N) of positive cases is indicated for each variable. Hazard Ratio, 95% Confidence Interval and Log-rank p-value are reported for each variable. In red bold are depicted all significant variables after BH correction.
*≤0.05; **≤0.01;***≤0.001;****≤0.0001

Supplementary materials

S.1

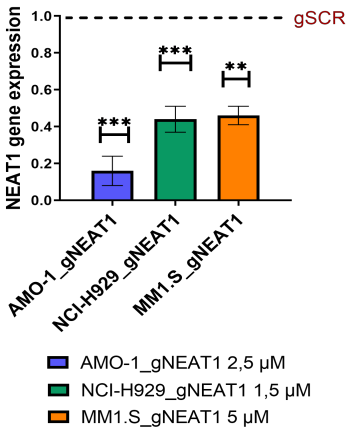

Supplementary figure 1 (S.1). NEAT1 silencing in MM cells. Quantitative real-time PCR of NEAT1 in AMO-1, NCI-H929 and MM1.S after NEAT1 KD (gNEAT1), compared to the scramble condition (96 hours of gapmeR delivery). NEAT1 expression was expressed as 2-ΔΔCt relative to thescramble gapmer (gSCR) at the same timepoint (n = 3).

S.2A S.2B

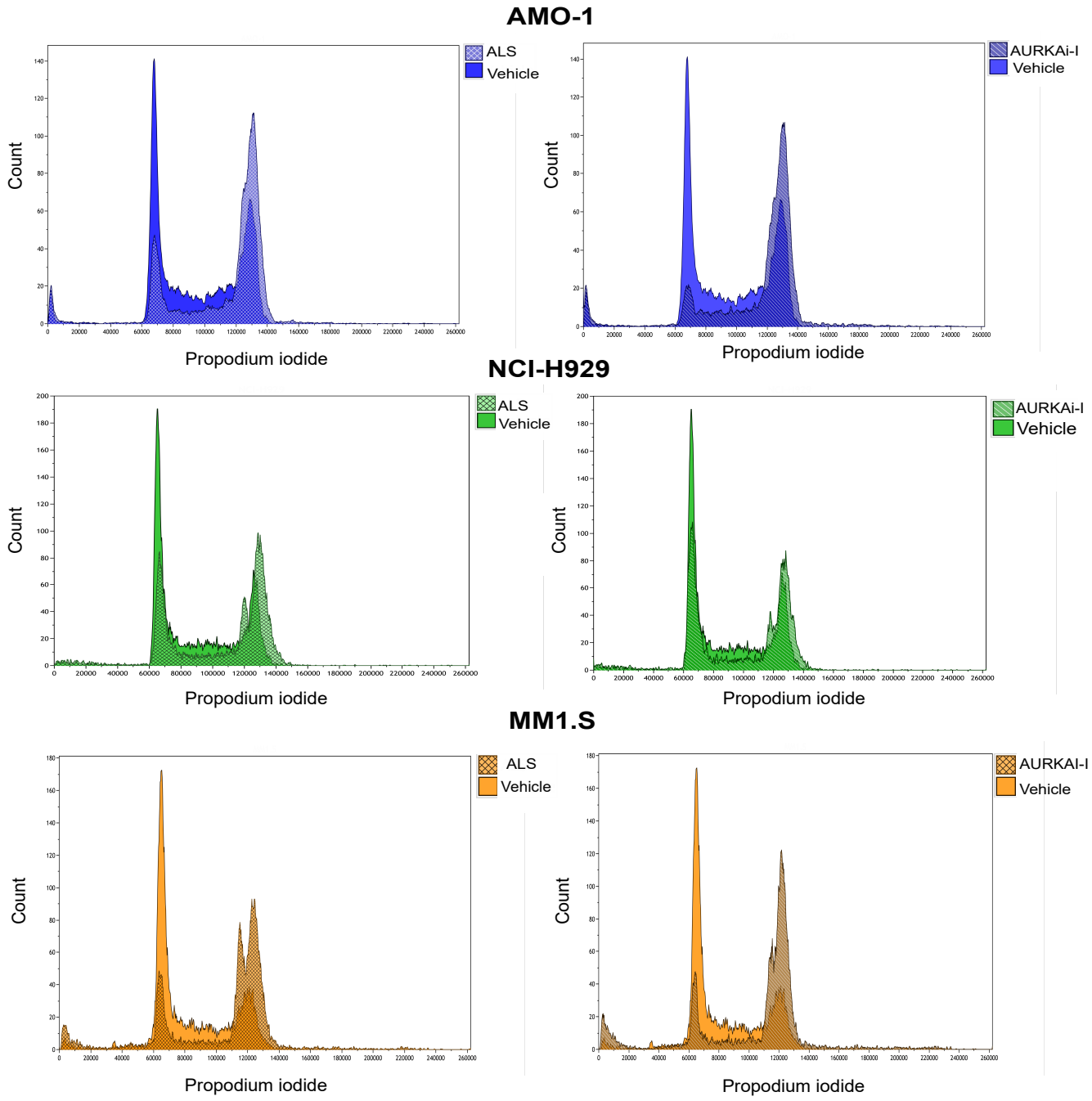

Supplementary figure 2. Effect of AURKA inhibition on cell cycle. Representative cell cycle profiles obtained through FACS analysis, of AMO-1, NCI-H929, MM1.S cells after 24 hours of Alisertib (**S.2A**) and AURKAi-I (**S.2B**) tretaments..

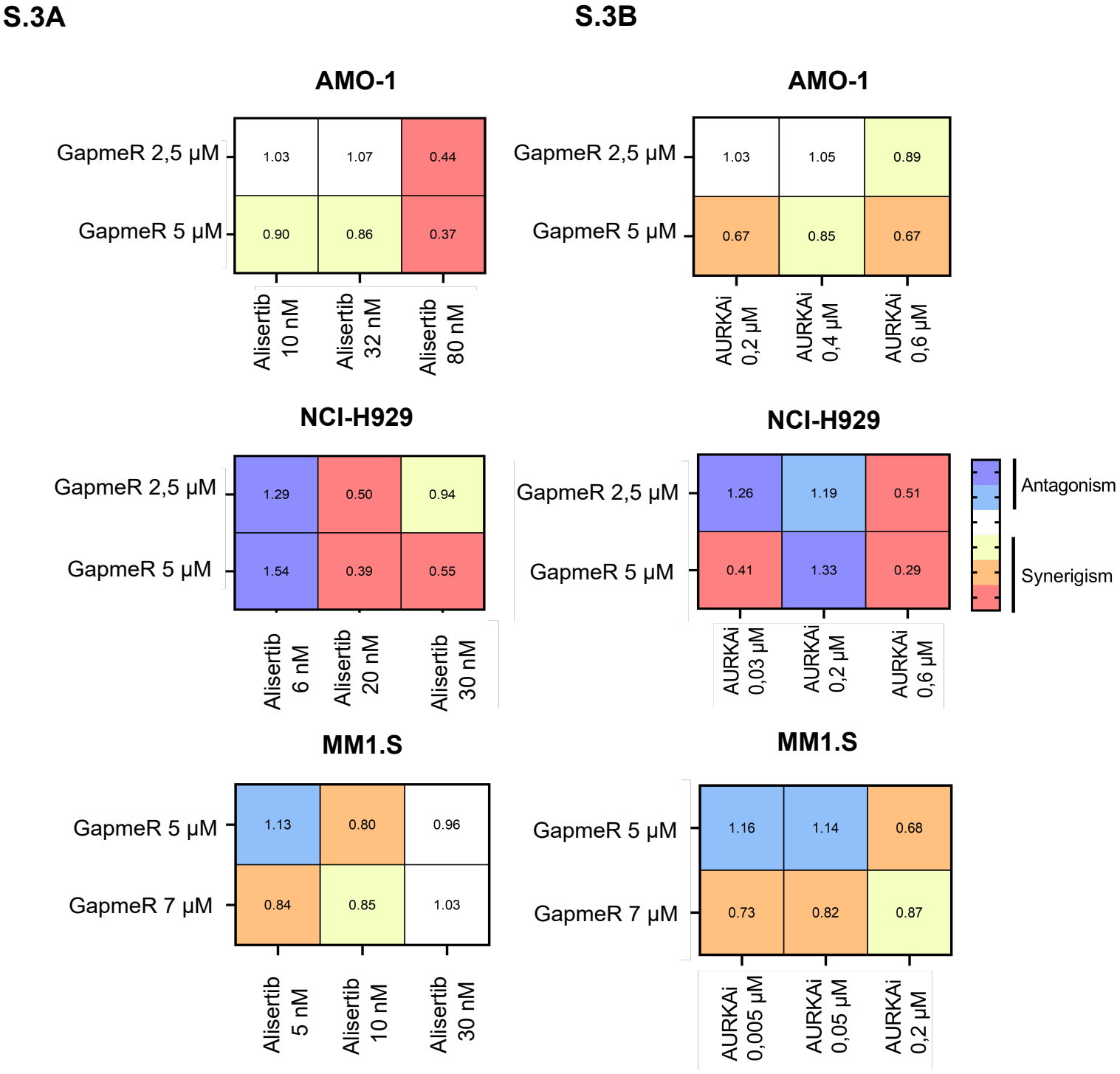

Supplementary figure 3. Synergy assessment. Combination matrix showing combination indexes (CI) resulting from combinatorial treatments of AMO-1,NCI-H929, MM1.S with GapmeR targeting total NEAT1 and Alisertib (**S.3A**) and AURKAi-I (**S.3B**) (3-day time point).

S.4

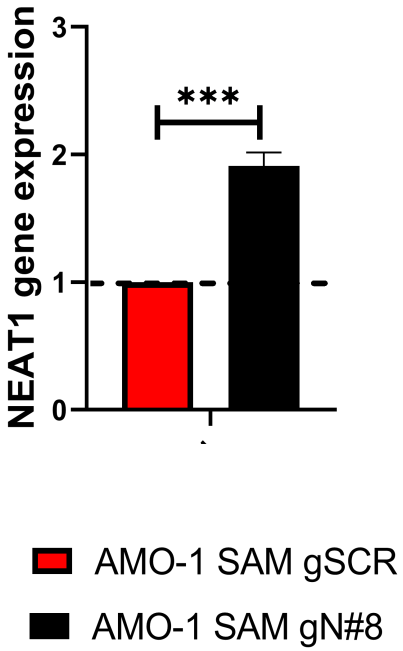

Supplementary figure 4 (S.4). NEAT1 transactivation in AMO-1 SAM gN#8 cell line.
Quantitative real time PCR showing NEAT1 expression level in AMO-1 SAM cells.
NEAT1 expression was expressed as 2^-ΔΔCt.
Satistical significance was measured with Student's t test.

S.5A

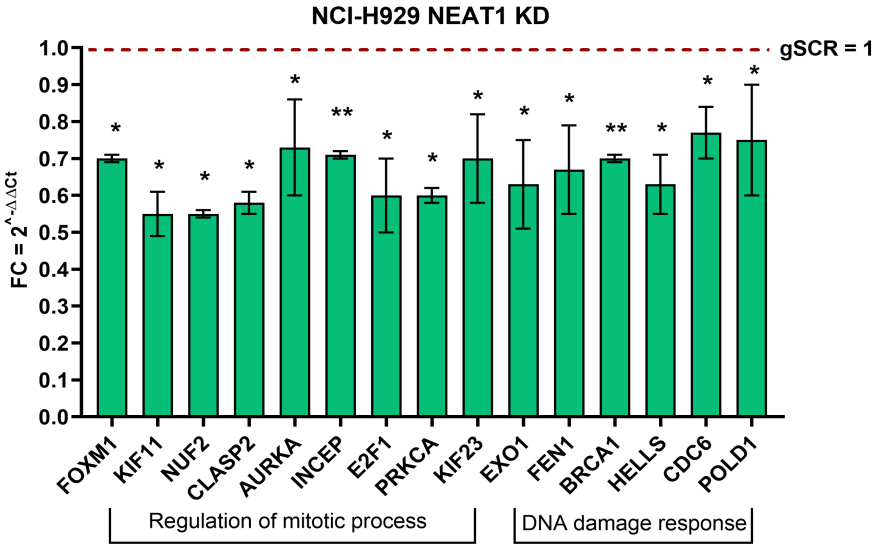

S.5B

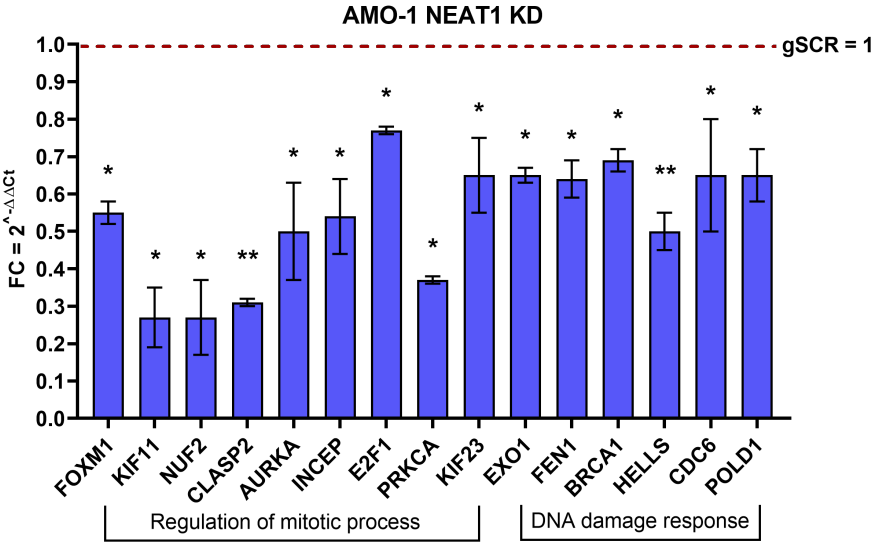

Supplementary figure 5. **Molecular validation of the most significant down-regulated genes in NEAT1 silenced cells.** qRT-PCR validation of differently expressed genes invovled in spindle assembly,mitotic regulation and DNA processes in NCI-H929 (**S.5A**) and AMO-1 silenced for NEAT1 expression (**S.5B**) following gNEAT1 delivery, compared to scramble condtion. (gSCR =1). Statistical significance was measured with Student's t test.

S.6

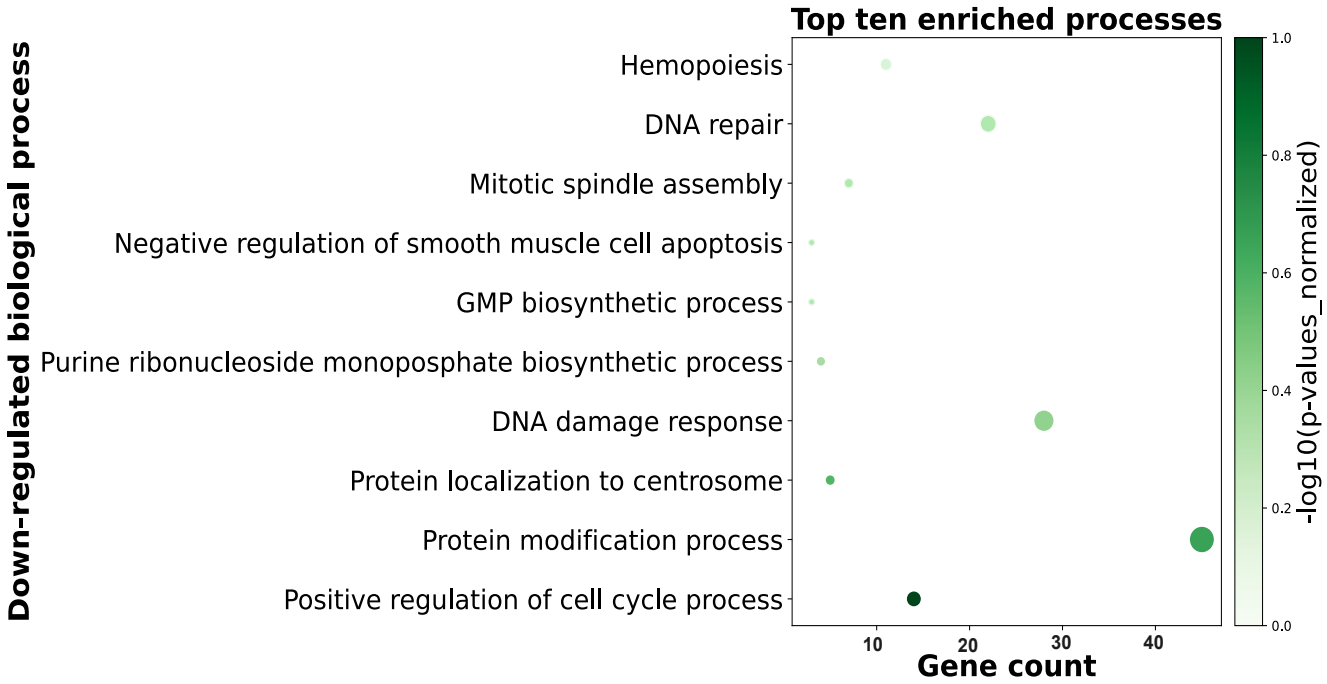

Supplementary figure 6 (S.6) Gene expression profiling data. Dot plot of the top ten down-regulated significant biological processes obtained in NCI-H929 NEAT1 KD cells following gNEAT1 delivery.

S.7

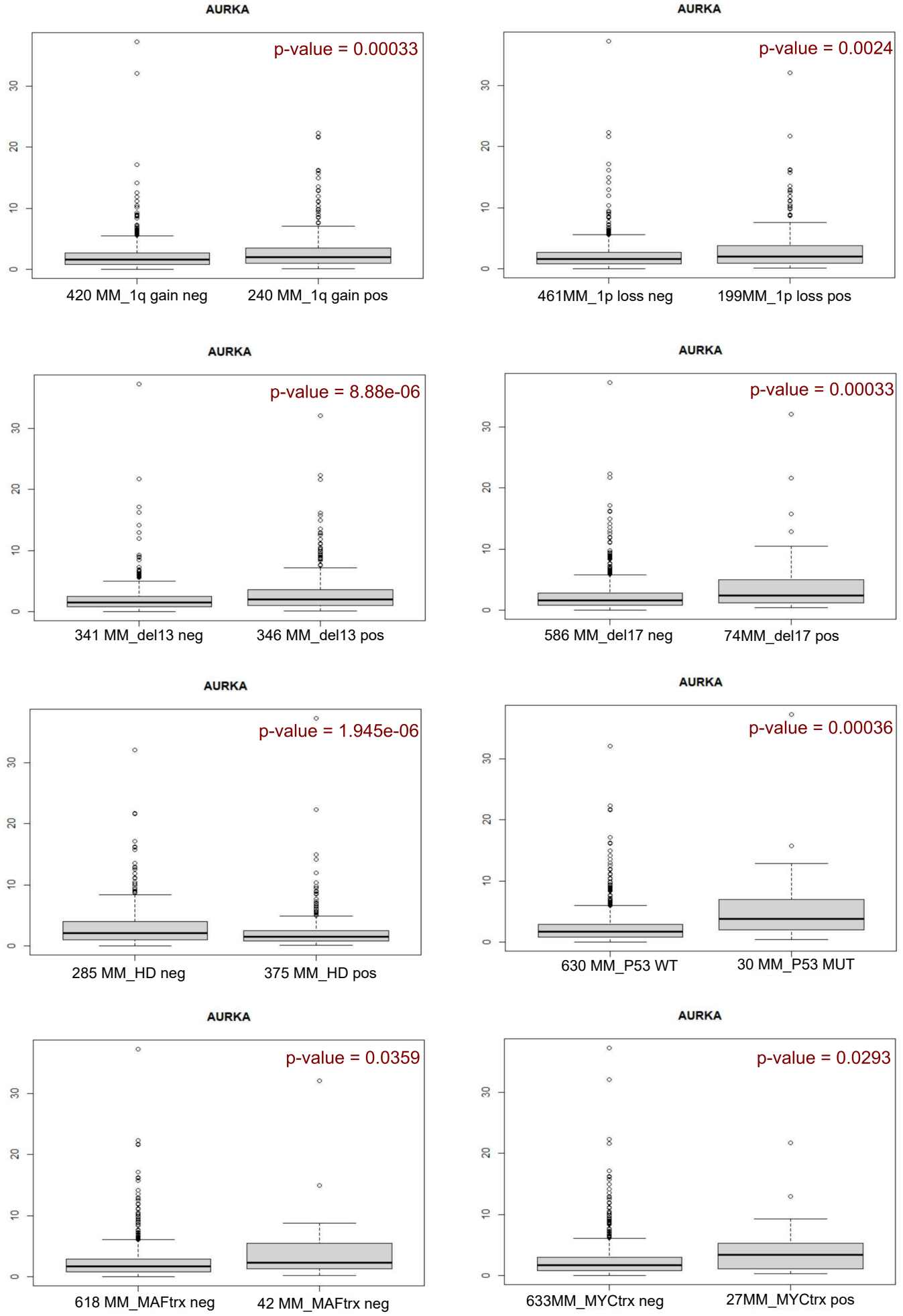

Supplementary figure 7 (S.7). Boxplots showing significant differences in AURKA expression in 660MM cases stratified according to the presence of 1q-gain, 1p-loss, del(13q), del(17p), hyperdiploidy (HD), TP53 alterations, MAF and MYC translocation (respectively MAFtrx, MYCtrx). or each plot, differential expression was tested by Wilcoxon rank-sum test with continuity correction. P-values were corrected by BH adjustment.

S.8A

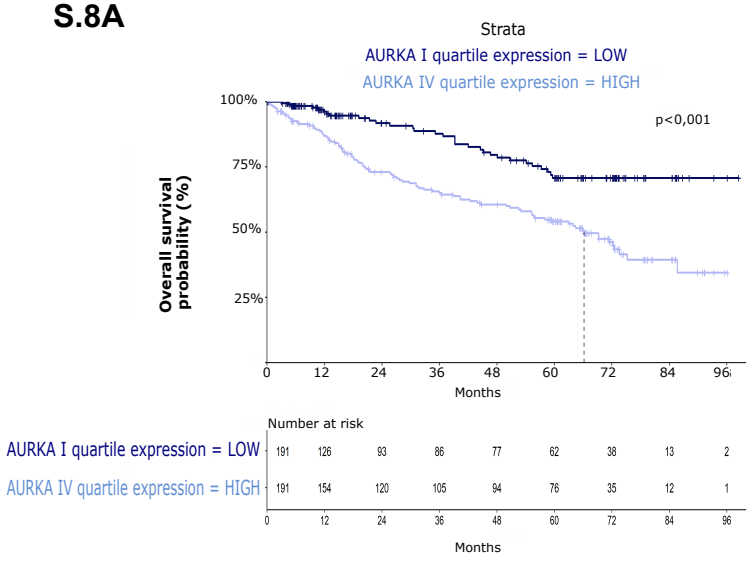

S.8B

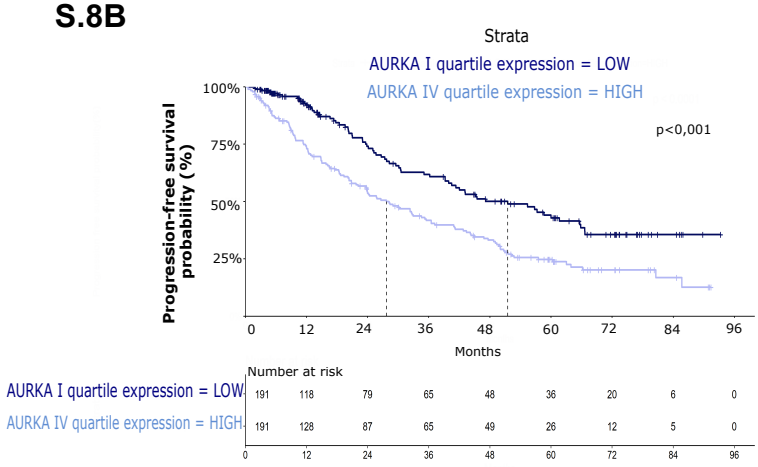

Supplementary figure 8. Survival analysis. Overall survival **(S.8A)** and progression-free survival **(S.8B)** probability calculated in the CoMMpass dataset which includes 761 patients with MM, stratified in high and low AURKA expression groups, according to quartile, across the dataset.
Log-rank test p-value measuring the global difference between survival curves and number of samples at risk in each group across time is reported

S.9A

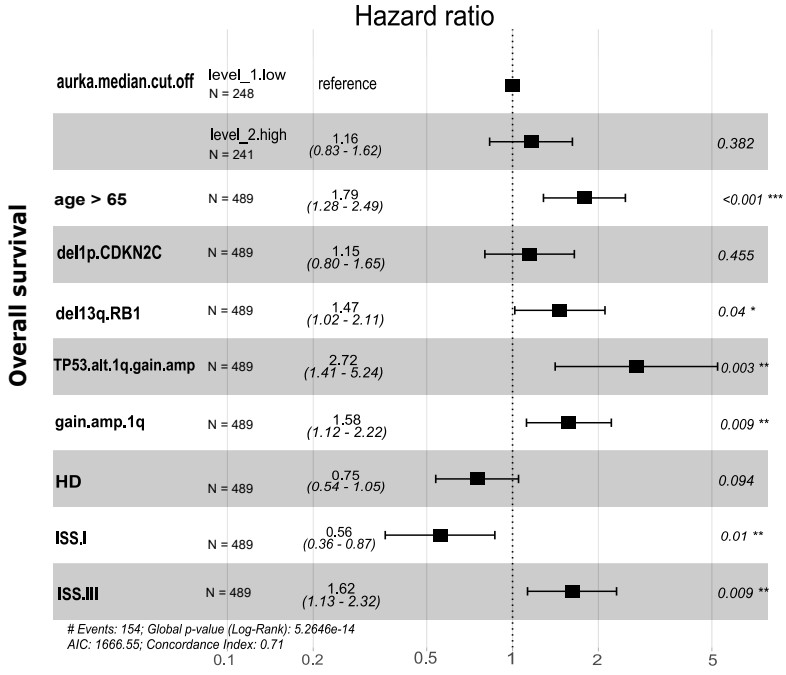

S.9B

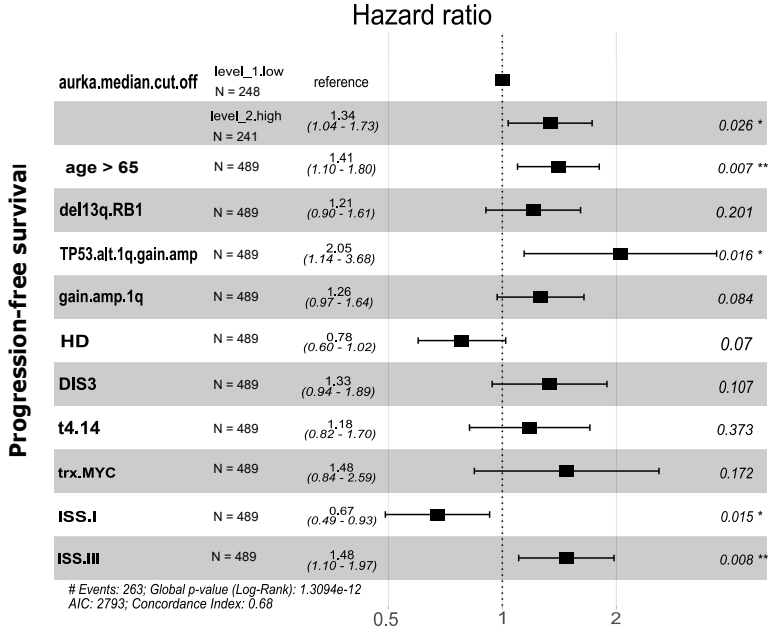

Supplementary figure 9. Multivariate analysis. Forest plots of Cox regression multivariate analyses considering all features with adjusted -value <0.05 in univariate analysis regarding to overall survival (**S.9A**) and progression-free survival (**S.9B**), in 489 patients with MM from the CoMMpass cohort.The hazard ratio, 95% confidence interval and P-value are reported or each variable. A global log-rank P-value is reported for each analysis

S.10

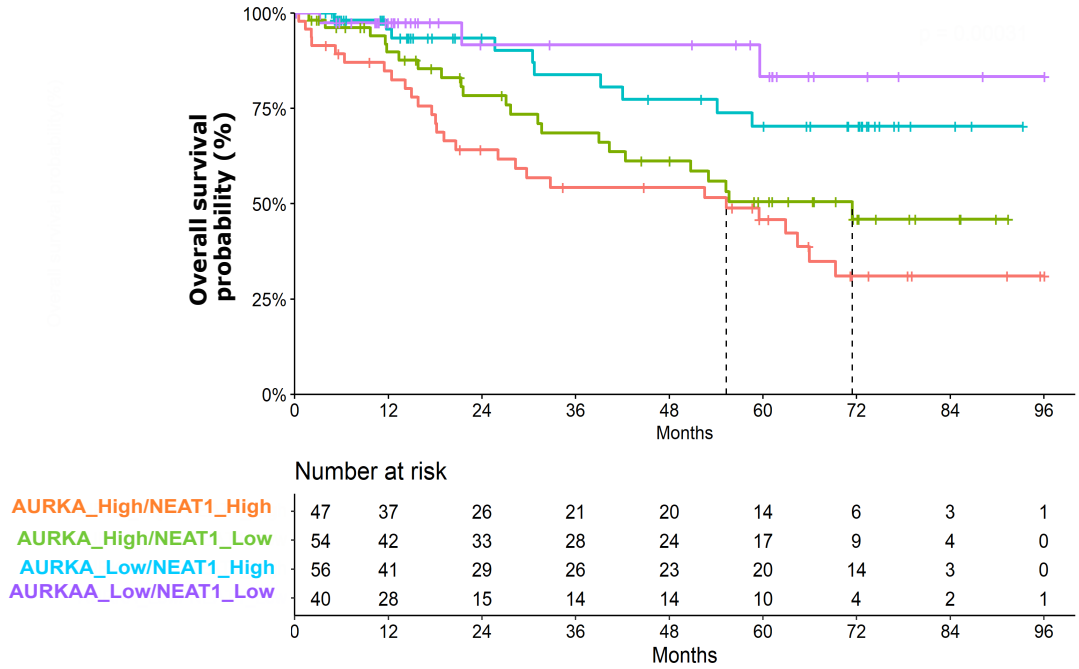

p value	AURKA_High/NEAT1_High	AURKA_High/NEAT1_Low	AURKA_Low/NEAT1_High
AURKA_High/NEAT1_Low	0,2064	-	-
AURKA_Low/NEAT1_High	0,0028	0,065	-
AURKA_Low/NEAT1_Low	0,0028	0,0226	0,2939

Supplementary figure 10 (S.10). Effects of AURKA and NEAT1 expression on MM patients survival. Kaplan-Meier survival curves of 761 patients stratified into four molecular groups based on NEAT1 and AURKA expression, according to quartile, across the CoMMpass dataset. Statistical significance between each curve was reported